Atmos. Meas. Tech., 4, 463–483, 2011
www.atmos-meas-tech.net/4/463/2011/
doi:10.5194/amt-4-463-2011

Atmospheric Measurement Techniques

MERIS albedo climatology for FRESCO+ O_2 A-band cloud retrieval

C. Popp[1], P. Wang[2], D. Brunner[1], P. Stammes[2], Y. Zhou[1], and M. Grzegorski[3]

[1]Empa, Swiss Federal Laboratories for Materials Science and Technology, Dübendorf, Switzerland
[2]Royal Netherlands Meteorological Institute (KNMI), De Bilt, The Netherlands
[3]Max-Planck-Institute for Chemistry, Mainz, Germany

Received: 23 September 2010 – Published in Atmos. Meas. Tech. Discuss.: 27 October 2010
Revised: 22 February 2011 – Accepted: 3 March 2011 – Published: 8 March 2011

Abstract. A new global albedo climatology for Oxygen A-band cloud retrievals is presented. The climatology is based on MEdium Resolution Imaging Spectrometer (MERIS) Albedomap data and its favourable impact on the derivation of cloud fraction is demonstrated for the FRESCO+ (Fast Retrieval Scheme for Clouds from the Oxygen A-band) algorithm. To date, a relatively coarse resolution ($1° \times 1°$) surface reflectance dataset from GOME (Global Ozone Monitoring Experiment) Lambert-equivalent reflectivity (LER) is used in FRESCO+. The GOME LER climatology does not account for the usually higher spatial resolution of UV/VIS instruments designed for trace gas remote sensing which introduces several artefacts, e.g. in regions with sharp spectral contrasts like coastlines or over bright surface targets. Therefore, MERIS black-sky albedo (BSA) data from the period October 2002 to October 2006 were aggregated to a grid of $0.25° \times 0.25°$ for each month of the year and for different spectral channels. In contrary to other available surface reflectivity datasets, MERIS includes channels at 754 nm and 775 nm which are located close to the spectral windows required for O_2 A-band cloud retrievals.

The MERIS BSA in the near-infrared compares well to Moderate Resolution Imaging Spectroradiometer (MODIS) derived BSA with an average difference lower than 1% and a correlation coefficient of 0.98. However, when relating MERIS BSA to GOME LER a distinctly lower correlation (0.80) and enhanced scatter is found. Effective cloud fractions from two exemplary months (January and July 2006) of Scanning Imaging Absorption Spectrometer for Atmospheric Chartography (SCIAMACHY) data were subsequently derived with FRESCO+ and compared to those from the Heidelberg Iterative Cloud Retrieval Utilities (HICRU) algorithm. The MERIS climatology generally improves FRESCO+ effective cloud fractions. In particular small cloud fractions are in better agreement with HICRU. This is of importance for atmospheric trace gas retrieval which relies on accurate cloud information at small cloud fractions. In addition, overestimates along coastlines and underestimates in the Intertropical Convergence Zone introduced by the GOME LER were eliminated. While effective cloud fractions over the Saharan desert and the Arabian peninsula are successfully reduced in January, they are still too high in July relative to HICRU due to FRESCO+'s large sensitivity to albedo inaccuracies of highly reflecting targets and inappropriate aerosol information which hampers an accurate albedo retrieval. Finally, NO_2 tropospheric vertical column densities and O_3 total columns were derived with the FRESCO+ cloud parameters from the new dataset and it is found that the MERIS BSA climatology has a pronounced and beneficial effect on regional scale. Apart from FRESCO+, the new MERIS albedo dataset is applicable to any cloud retrieval algorithms using the O_2 A-band or the O_2-O_2 absorption band around 477 nm. Moreover, the by-product of BSA at 442 nm can be used in NO_2 remote sensing and the BSA at 620 nm, 665 nm, and 681 nm could be integrated in current H_2O retrievals.

1 Introduction

Accurate cloud information is an important prerequisite for the retrieval of atmospheric trace gases from spaceborne UV/VIS sensors. Errors in the estimated cloud fraction and cloud height (pressure) result in erroneous air mass factors and thus lead to inaccuracies in the vertical column densities of the retrieved trace gas. For example, Boersma et al. (2004) estimated in their tropospheric NO_2 error analysis average uncertainties in the tropospheric air mass factor as large as 30% due to cloud fraction and up to 10% due to cloud top pressure inaccuracies. In addition, the majority of the

Correspondence to: C. Popp
(christoph.popp@empa.ch)

UV/VIS instruments have a rather coarse spatial resolution which increases the probability of cloud contamination in the sensor's field of view (e.g., Krijger et al., 2007). Several algorithms for the retrieval of cloud fraction and cloud pressure from UV/VIS sensors have been developed, depending on the instrument's spectral characteristic. Some take advantage of the oxygen absorption in the O_2 A-band around 760 nm (e.g. Kuze and Chance, 1994; Koelemeijer et al., 2002; Wang et al., 2008; Kokhanovsky et al., 2006), absorption in the O_2-O_2 band around 477 nm (e.g. Acarreta et al., 2004), O_2 absorption in several bands (Wagner et al., 2008), Raman scattering (Vasilkov et al., 2008), or of a combination of measurements from the Polarisation Measurement Devices (PMD) with measurements either in the O_2-γ-band (Grzegorski et al., 2006) or in the O_2 A-band (Loyola et al., 2007). Since O_2 is a well-mixed gas, O_2 A-band retrieval algorithms utilize the varying depth of the oxygen absorption as a function of the oxygen amount above the cloud (Koelemeijer et al., 2002).

In ESA's TEMIS (Tropospheric Emission Monitoring Internet Service) project, the FRESCO+ (Fast Retrieval Scheme for Clouds from the Oxygen A-band) cloud retrieval is applied to SCIAMACHY (SCanning Imaging Absorption SpectroMeter for Atmospheric ChartograpHY) (Bovensmann et al., 1999) and Global Ozone Monitoring Experiment (GOME(-2)) (Burrows et al., 1999; Munro et al., 2006) data to derive effective cloud fraction and cloud pressure for each pixel. FRESCO+ (Wang et al., 2008) uses measured top-of-atmosphere (TOA) reflectance in three wavelength windows inside and outside of the O_2 A-band (at 758–759 nm, 760–761 nm, and 765–766 nm). Effective cloud fraction and cloud pressure are retrieved by minimizing the difference between TOA reflectance from radiative transfer calculations and the measured TOA reflectance. With regard to the radiative transfer simulations, FRESCO+ relies on a surface reflectance climatology based on GOME Lambert-equivalent reflectivity (LER) acquired between June 1995 and December 2000 (Koelemeijer et al., 2003). However, the relatively coarse resolution ($1^\circ \times 1^\circ$) of the GOME LER database often inadequately represents surface reflectivity in the instantaneous field of view of recent UV/VIS instruments (e.g. ground pixel size of $30 \times 60\,km^2$ for SCIAMACHY) thereby introducing several artefacts in cloud and trace gas retrievals. For example in regions with strong spatial gradients of reflectance like coastlines (cf. Fig. 1), the surface albedo over land is often underestimated which results in an overestimation of the effective cloud fraction. In addition, land use changes during the past decade potentially introduce further inaccuracies in the cloud parameter retrieval.

For these reasons, we test the substitution of the GOME LER climatology in FRESCO+ with a land surface albedo climatology compiled for every month from MEdium Resolution Imaging Spectrometer (MERIS) Albedomap data (Muller, 2008) covering the period October 2002 to October 2006. Contrary to other available BRDF/albedo products, e.g. from the Moderate Resolution Imaging Spectroradiometer (MODIS, Schaaf et al., 2002), the MERIS dataset provides albedo values at 754 nm and 775 nm located close to both sides of the O_2 A-band as required by FRESCO+. Further, the increased spatial resolution of the MERIS product in comparison to the GOME LER dataset ($0.05^\circ \times 0.05^\circ$, herein aggregated to $0.25^\circ \times 0.25^\circ$) allows to better account for the typical pixel size of UV/VIS sensors. The aim of this study is to describe and assess (i) the compilation and quality of the MERIS albedo climatology, (ii) the differences to the GOME LER climatology, and (iii) to demonstrate the enhancements in the FRESCO+ O_2 A-band cloud retrieval after integration of the MERIS albedo climatology based on SCIAMACHY data.

2 FRESCO+

The basic FRESCO algorithm is described in detail in Koelemeijer et al. (2002) and the updated FRESCO+ in Wang et al. (2008). Cloud retrieval in the O_2 A-band takes advantage of the larger reflectance of (subpixel) clouds in the continuum window (758–759 nm) as well as the varying depth of the oxygen absorption at 760 nm and 765 nm as a function of cloud height and cloud optical thickness. Effective cloud fraction and cloud pressure are inverted by minimizing the difference between radiative transfer simulations of TOA reflectance and the measured TOA reflectance by applying the Levenberg-Marquart nonlinear least squares method. Following the independent pixel assumption, the (simulated) TOA reflectance can be expressed as the sum of terms containing the reflectance from the cloudy part and from the cloud-free part of the pixel:

$$R_{\mathrm{sim}} = c A_{\mathrm{c}} T_{\mathrm{c}} + (1-c) A_{\mathrm{s}} T_{\mathrm{s}} + c R_{\mathrm{c}} + (1-c)\ R_{\mathrm{s}} \qquad (1)$$

where subscript c indicates cloud related and subscript s surface related parameters. Hence, A_{c} and A_{s} are the cloud and surface albedo, c is the effective cloud fraction, T_{s} and T_{c} the direct transmissions along the photon path (from the sun to surface or cloud and back to TOA), and R_{c} and R_{s} the single Rayleigh scattering reflectance including O_2 absorption between the cloud (surface) and TOA. The transmissions T_{c} and T_{s} depend on the solar zenith angle and the viewing zenith angle and include O_2 absorption and Rayleigh extinction. With the exception of c, all parameters in Eq. (1) are wavelength dependent. Cloud pressure is a function of the depth of the O_2 A-band. The radiative transfer calculations include an assumed cloud albedo of 0.8, a mid-latitude summer atmosphere profile (Anderson et al., 1986), surface height from the GTOPO30 digital elevation model (from the US Geological Survey's EROS data center), surface albedo from a climatology based on GOME measurements, and TOMS (Total Ozone Mapping Spectrometer) surface albedo (Herman and Celarier, 1997) to estimate snow or ice covered areas. From a computational perspective, a transmission database

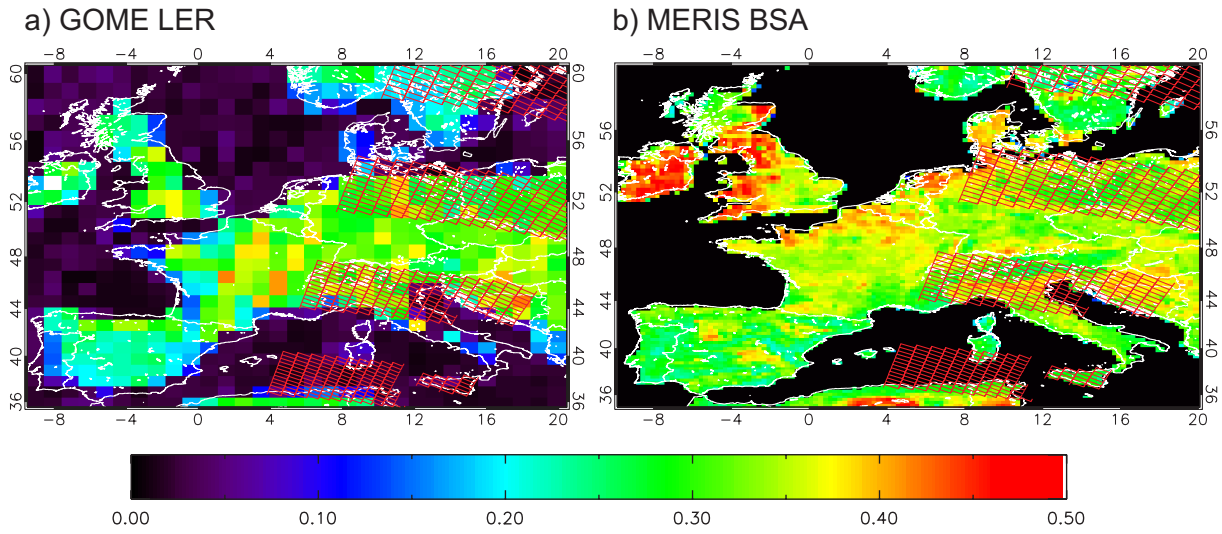

Fig. 1. Comparison between GOME LER with a spatial resolution of 1° × 1° (758 nm) and MERIS BSA (754 nm) with a spatial resolution of 0.25° × 0.25° for the month of July over Europe. Superimposed in red are the outlines of the SCIAMACHY pixels (30 × 60 km^2) for an orbit from 14 July 2006. Note that no albedo values over ocean are available for the MERIS data.

is pre-calculated by line-by-line radiative transfer calculations, convoluted with the slit function of SCIAMACHY (Wang et al., 2008).

The FRESCO algorithm/software has undergone several improvements and different validations. In its first version (Koelemeijer et al., 2002), the surface albedo of ocean was assumed to be constant at 0.02 and the surface albedo of land was estimated from minimum reflectivity data from two months of GOME observations on a grid of 2.5° × 2.5° resolution. Subsequently, Koelemeijer et al. (2003) compiled a climatology of Lambert-equivalent reflectivity (LER) based on several years of GOME data on a monthly basis and a spatial resolution of 1° × 1°. The spectrum corresponding to the minimum LER at 670 nm per month and grid cell is stored in the dataset. The surface LER used in FRESCO are at 758 nm and 772 nm. Fournier et al. (2006) found an overestimation of effective cloud fraction over deserts which they attributed to (absorbing) desert dust aerosols and corrected this effect by increasing the monthly surface albedo by (empirically found) 20% at desert locations with a monthly six-year average of the Absorbing Aerosol Index (AAI) from GOME larger than one. Finally, Wang et al. (2008) added single Rayleigh scattering (last two terms in Eq. 1) in the radiative transfer calculations thereby mainly improving the estimation of cloud pressure for less cloudy pixels which is of special interest for trace gas retrieval in the troposphere.

FRESCO+ retrieves an effective cloud fraction which describes the fraction of an optically thick Lambertian cloud with a fixed albedo of 0.8 that results in the same TOA radiance as the real cloud. Thus, the effective cloud fraction is a radiometric equivalent cloud fraction. This concept has been proven useful for trace gas remote sensing applications (Koelemeijer et al., 2002; Stammes et al., 2008) and estimated errors introduced to trace gas retrievals are usually quite small (and minimal for a fixed cloud albedo of 0.8) when compared to scattering cloud models (Stammes et al., 2008). In general, the reflectance of clouds is directional dependent. This anisotropy is not (and does not have to be) included in the FRESCO+ algorithm because the effective cloud fraction is used to correct trace gas measurements for the cloud reflectance in the same pixel under the same viewing and illumination angles. Therefore, the effective cloud fraction represents the pixel-averaged cloud reflectance under the actual viewing and illumination conditions. However, it should be emphasized that the effective cloud fraction is not directly comparable to (and usually smaller than) the geometric cloud fraction like e.g. reported by synoptic observations of weather services or derived applying other algorithms (e.g. Loyola, 1998; Kokhanovsky et al., 2009; Schlundt et al., 2011). The retrieval of cloud information is seriously hampered over snow-contaminated surfaces because it is difficult to separate the measured and the cloud's radiometric signal over surfaces which exhibit a similar reflection as the cloud itself (e.g., Tuinder et al., 2004). It further follows from Eq. (1) that the effective cloud fraction becomes highly sensitive to errors in the surface albedo when the surface albedo approaches the cloud albedo (Koelemeijer et al., 2002). Therefore, over snow/ice no cloud fraction is retrieved but a scene albedo and scene pressure are retrieved.

3 MERIS albedo database

3.1 Albedomap data

The European Space Agency (ESA) initiated the Albedomap project with the aim to create a global land surface albedo dataset from MERIS measurements. The resulting white-sky and black-sky albedo data are available from http://www.brockmann-consult.de/albedomap/ created for periods of 16 days or one month, respectively. Black-sky albedo (BSA) is the ratio of the upwelling to downwelling direct radiative flux (often also called the directional hemispherical reflectance), white-sky albedo is the ratio of the upwelling to downwelling (isotropic) diffuse flux (bihemispheric reflectance). Global surface albedo maps are available for the period July 2002 to November 2006 on a grid of $0.05° \times 0.05°$. However, due to quality issues in the August and September 2002 data, we compile the climatology based on data from October 2002 onward. The albedo maps are spatially complete with the exception of regions affected by polar darkness and some patches in adjacent regions between approximately 55° N and 60° N in Siberia and Canada for the months of October, November, and December. The cause of the latter artefact is currently not known. White- and black-sky albedos are available for 13 out of 15 spectral bands of MERIS between 412 nm and 885 nm[1]. The MERIS channels at 754 nm and 775 nm are located spectrally close to both sides of the O_2 A-band and are therefore of special interest in this study. A detailed description of the derivation of surface albedo from MERIS data can be found in Muller (2008). In brief, top-of-atmosphere MERIS Level2 reflectance is first cloud-screened and corrected for aerosol extinction (Schroeder et al., 2005) providing the MERIS Level 2 SDR (surface directional reflectance). The cloud detection is based on simulated radiances representing the natural variability of cloud and surface spectral properties which train an artificial neural network that converts the MERIS measurements into likelihood of cloudiness (Preusker et al., 2008). A post-processing is subsequently applied including several spectral and temporal tests and cloud edge detection in order to improve cloud shadow detection, discrimination between cloud and snow/ice and the detection of thin clouds. The aerosol correction uses aerosol optical depth and Angstroem coefficient derived from the daily MODIS aerosol product (Kaufman and Tanré, 1998) or from the the Global Aerosol Data Set (GADS) climatology (Koepke et al., 1997). The daily SDR of a 16-day period are subsequently averaged to the resolution of 0.05° in accordance to the MODIS Climate Modelling Grid BRDF (bi-directional reflectance distribution function) product (MOD43C, Schaaf et al., 2002). A magnitude inversion technique is then applied to the shape of the MODIS BRDF using the MERIS SDR. Black-sky and white-sky albedo are finally obtained by integrating the corresponding BRDF over the hemisphere, in case of the black-sky albedo for the mean solar zenith angle of the corresponding 16-days periods (Muller, 2008). In addition, a monthly product is generated by averaging the 16-day data weighted by the number of days falling in the specific month. It is emphasized that the MERIS albedo data depends on the quality of the MODIS BRDF parameters. These parameters could be originating from a full inversion or in case of poor sampling from a predetermined global and season-dependent database of BRDF parameters characteristical for different land cover types (Schaaf et al., 2002). The Albedomap dataset provides albedo values for solar zenith angles up to around 80° as well as for land surfaces and shallow water areas but not for deep ocean pixels.

[1] i.e. 412 nm (bandwidth 10 nm), 442 nm (10 nm), 490 nm (10 nm), 510 nm (10 nm), 560 nm (10 nm), 620 nm (10 nm), 665 nm (10 nm), 681 nm (7.5 nm), 709 nm (10 nm), 754 nm (7.5 nm), 775 nm (15 nm), 865 nm (20 nm), 885 nm (10 nm)

3.2 Compilation of the MERIS BSA climatology

Using the Albedomap data we compiled a monthly climatology by averaging over the period 2002–2006. Black-sky albedo is chosen as the reflectance quantity of interest for reasons explained in Sect. 4.1. The processing is straightforward and the following steps are performed for each spectral channel:

1. All valid BSA pixels for a particular month of the year from the $0.05° \times 0.05°$ database are collected in boxes of $0.25° \times 0.25°$. The MODIS monthly snow product MOD10CM (Hall et al., 2002) on a grid of 0.05° resolution is used to reject snow contaminated pixels. If a box contains less than 25 out of 100 (25 pixels × 4 years) possible valid and snow/ice-free pixels it is regarded unreliable because of e.g. too much snow coverage or corrupted data. In this case the grid cell is left empty and filled later.

2. If the MODIS snow product indicates that more than 25% of the valid BSA pixels are snow-free, the median of all snow-free black-sky albedo values is stored in the corresponding grid cell. We choose the median BSA to reduce the impact of possible outliers like undetected snow.

3. If the MODIS snow product indicates that more than 75% of all valid pixels have a snow fraction larger than 0.75, the median BSA of all these snow covered pixels and the corresponding snow fraction are stored.

4. For grid cells with more than 25 valid pixels but not filled during steps 2 and 3, the median and the corresponding snow fraction are stored and these grid cells are flagged as (subgrid) snow-contaminated.

5. Empty grid cells (e.g. due to polar darkness) are filled with the value from the closest month and a corresponding flag is set.

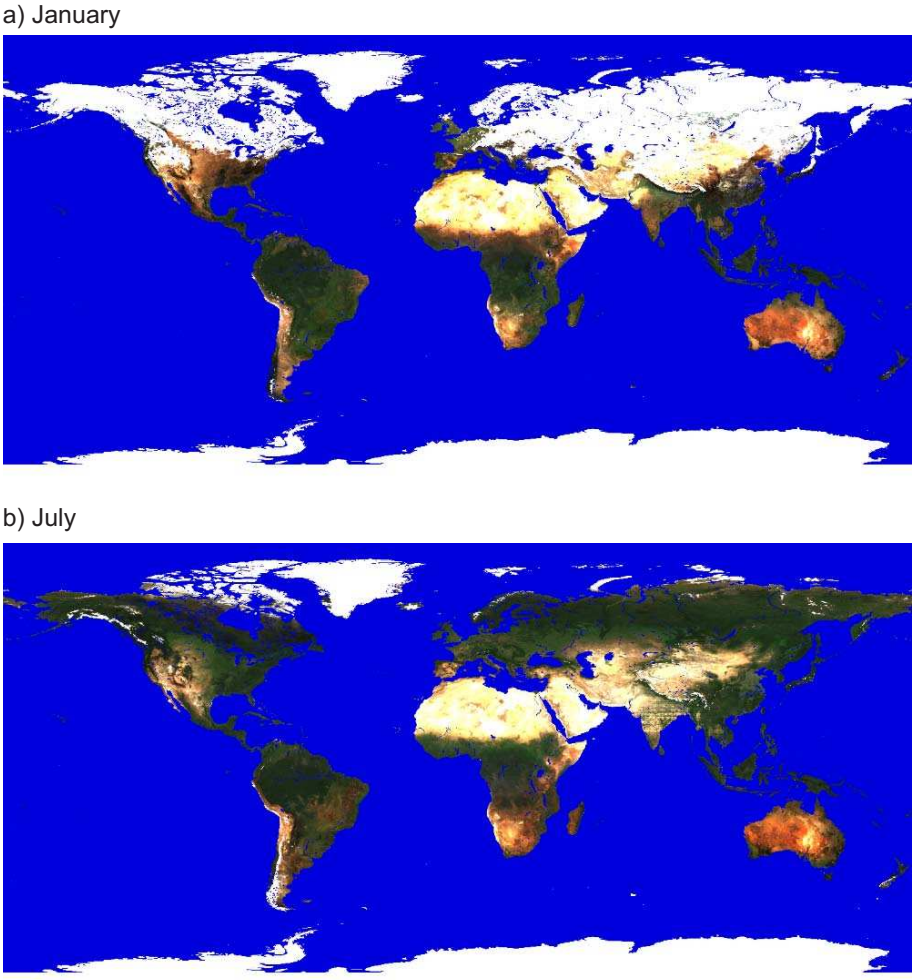

Fig. 2. RGB composites for the MERIS BSA dataset for January and July (R: 665 nm, G: 650 nm, B: 490 nm). Oceans and larger inland water bodies are filled with an artificial blue color.

6. Water pixels are finally filled (or replaced in case of shallow water near the shores) by the LER from the GOME database and a corresponding flag is set.

In contrast to climatologies built from lower level data (e.g., Kleipool et al., 2008; Koelemeijer et al., 2003) we do not have to deal with cloud masking because the database is already sufficiently cloud screened (Preusker et al., 2008). Therefore, the median is applied in the second step to minimize the influence of potential outliers, e.g. snow. Step 4 leads to subgrid snow-contaminated pixels in the dataset which are flagged but might be used for some applications. Step 5 is mainly performed to obtain a spatially complete dataset. A majority of missing pixels can be assigned to unfavourable illumination conditions, e.g. during winter at high latitudes.

Global RGB composites of the resulting climatology are presented in Fig. 2 for the months of January and July. An artificial blue color is assigned to water pixels. The differences between winter and summer are well depicted. Snow coverage in the northern hemisphere is widespread in January and characterized by high reflectivity in the three bands (R: 665 nm, G: 560 nm, B: 490 nm) used to build the RGB. In addition, the greening of vegetation e.g. in North America or the Sahel as well as some changes toward arid conditions during summer, e.g. in Spain, are well detectable.

4 Results and discussion

4.1 Comparison to GOME LER and MODIS BSA

We compare our MERIS black-sky albedo dataset with two existing albedo climatologies, namely the spatially complete MODIS black-sky (Moody et al., 2008) and the GOME LER (Koelemeijer et al., 2003) datasets. It should be noted that black-sky albedo is not the same measure as the Lambert-equivalent reflectivity. BSA is the integral of the BRDF over

the entire hemisphere whereas the LER is derived from a much smaller range of viewing angles of the satellite's observation geometry (e.g., Kleipool et al., 2008). Further, the MERIS BSA (overpass at 10:00 LT – local time) are reported for the mean solar zenith angle of the 16-day periods which does not necessarily have to accord to the solar zenith angles of GOME data acquisition (overpass at 10:30 LT) that was used for the GOME LER. Finally, diffuse illumination is disregarded in the BSA whereas in reality some part of the illumination is usually diffuse (blue-sky albedo). However, we justify the use of black-sky albedo for FRESCO+ because (i) in FRESCO+, the albedo climatology is exclusively used to perform the radiative transfer calculations for the clear-sky part of the pixel (cf. Eq. 1); (ii) in clear-sky cases (only aerosol and Rayleigh scattering) diffuse irradiance around 760 nm is usually small compared to the direct irradiance; (iii) the black-sky albedo is generally very similar to the blue-sky albedo for moderate solar zenith angles (0°–50° as demonstrated in Liu et al., 2009) because the diffuse component decreases with decreasing solar zenith angle; and (iv) the "actual" (blue-sky) albedo is difficult to calculate because accurate knowledge about the atmospheric optical depth is required which is highly variable in space and time. Oleson et al. (2003) reported differences of not more than 2% between BSA and blue-sky albedo and less than 2.3% between BSA and WSA for different zonal averages.

4.1.1 GOME LER climatology

The GOME LER climatology is described in detail in Koelemeijer et al. (2003). In summary, the climatology provides LER in eleven spectral bands between 335 nm and 772 nm suitable for a wide range of applications (e.g. retrieval of trace gases or aerosols) derived from GOME measured spectra with a spatial resolution of $320 \times 40\,\mathrm{km}^2$. The minimum value at 670 nm of all the LER values falling in each $1^\circ \times 1^\circ$ grid cell per month acquired between June 1995 and December 2000 is stored in the data base. The minimum LER is expected to have the least cloud contamination. For the remaining ten channels, the corresponding values of the same spectrum are stored. Three correction steps are subsequently applied to account for remaining cloud effects over ocean, to remove (temporal) outliers, and to fill empty grid cells. The GOME LER database was evaluated by comparison to the TOMS climatology (Herman and Celarier, 1997) for the UV channel at 380 nm and biases in the order of ∼0.007–0.023 as well as standard deviations (σ) ∼0.02 were found and judged as satisfactory (Koelemeijer et al., 2003). Fournier et al. (2006) corrected the underestimation of the surface albedo over deserts by empirically found 20%. Herein, we exclusively use this updated GOME database. Figure 1 illustrates the differences between the GOME LER $1^\circ \times 1^\circ$ resolution and the MERIS $0.25^\circ \times 0.25^\circ$ resolution climatology for the month of July exemplified for a subset covering Europe. Superimposed in red are the outlines of the individual pixels of one SCIAMACHY orbit from 14 July 2006 where a valid vertical trace gas column could have been retrieved. Obviously, the level of detail is much more pronounced in the MERIS BSA data. Different landscape structures such as the Alpine mountain range can be much better observed in the MERIS map. Further, coastlines are distinctively better detectable in the MERIS BSA data, e.g. around the Iberian peninsula or along the African coast. It often appears in the GOME ($1^\circ \times 1^\circ$) dataset that grid cells along coastlines are filled with the ocean LER, e.g. Mediterranean islands like Corsica, Sardinia, Balearic islands, and to some extent Sicily are not captured at all. This mismatch can not only be assigned to GOME's coarser spatial resolution but can also originate from the selection criterion applied to create the GOME LER database. A grid cell covering land and ocean surfaces has a higher probability to be filled with the water spectra as the minimum value at 670 nm is selected where a majority of land surfaces are brighter than ocean. Also the southern part of Italy is strongly affected underlined by the much higher values in the MERIS BSA data than in the GOME LER data for this region. This misclassification can seriously hamper the cloud parameter retrieval. In addition, some larger differences of the BSA and LER values are occasionally detectable. For example, parts of Ireland, Great Britain or the Netherlands show distinctively higher values for MERIS BSA than for GOME LER.

4.1.2 MODIS black sky albedo

The MODIS BSA dataset is available at a resolution of one arc-minute and has been compiled from albedo data (MOD43B3, Schaaf et al., 2002) covering the years 2000 to 2004 (available from ftp://modis-atmos.gsfc.nasa.gov/L3LandSurfaceProducts). The MODIS data represents spatially complete snow-free albedo values derived with an ecosystem-dependent temporal interpolation technique that has an accuracy of ∼3%–8% (Moody et al., 2008). In order to compare the two datasets we averaged 15×15 pixels of each MODIS image to match the 0.25° resolution of our MERIS climatology. Further, the MODIS data is provided at a temporal resolution of 16 days. Therefore, we calculate mean values for each month in a similar way as for MERIS (cf. Sect. 3.2), i.e. as an average weighted by the number of days falling in the specific month. The performance of the MERIS BSA is assessed in the near-infrared (NIR) wavelength region which is of interest for cloud parameter retrieval in the O_2 A-band. With the exclusion of snow (and water), most natural land surfaces exhibit an enhanced reflectivity in the NIR, e.g. vegetated areas or arid regions. MODIS BRDF/albedo products are not available for the spectral region around the O_2 A-band. However, the MODIS channel at 858 nm is spectrally positioned close enough to the MERIS 865 nm channel to conduct the comparison there. The MERIS channels at 754 nm, 775 nm, and 865 nm are highly correlated. The first principal component

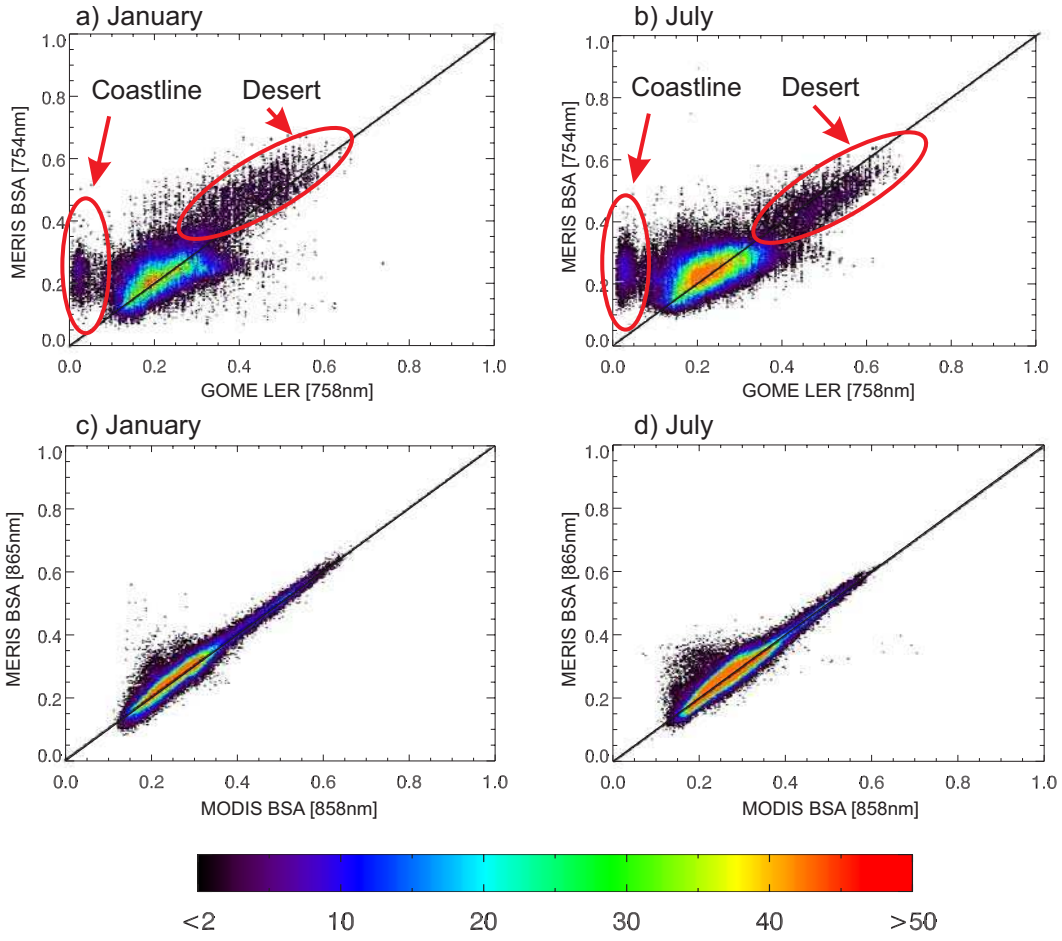

Fig. 3. Scatter density plots of MERIS BSA as a function of GOME LER and MODIS BSA for January and July for the NIR wavelength region. Only snow/ice-free grid cells over land are compared.

of the eigenvalues of the three channels accounts for more than 99.5% of the variance in the data suggesting that the MODIS-MERIS comparison provides valuable information about the quality of the MERIS channels at 754 nm and 775 nm. Finally, it should be noted that these two datasets are not completely independent since the MERIS Albedomap product uses MODIS derived aerosol parameters for atmospheric correction and BRDF parameters to infer the black- and white-sky albedo (cf. Sect. 3.1).

4.1.3 Statistical analysis

Scatter density plots of MERIS BSA (at 754 nm) vs. GOME LER (at 758 nm) for the months of January and July, respectively, are given in Fig. 3. Snow masked pixels are excluded from the comparison. The marked cluster detectable at GOME LER values lower than 0.05 and MERIS BSA between approximately 0.1 and 0.4 can be assigned to pixels along coastlines (cf. Fig. 4) where the contrast between ocean and land pixels is relatively large in the NIR. These pixels are apparently misclassified in the GOME LER database due to its relatively coarse spatial resolution and selection criteria (cf. Fig. 1). The second feature marked in Fig. 3 consists of pixels mostly from arid areas, like the Saharan desert. Obviously, the GOME LER is underestimated in January while MERIS BSA is slightly lower than GOME LER July in the desert grid cells. The scatter density plots also demonstrate that these areas belong to the brightest surfaces in the NIR (apart from snow which has been masked here). Accurate information about the reflectivity of those targets is of particular interest since FRESCO+ is especially sensitive to changes of large albedo values (cf. Eq. 1). The highest densities occur close to the bisecting line but the scatter is rather large.

The lower two scatter density plots in Fig. 3 illustrate MERIS BSA vs. MODIS BSA for the months of January and July. In general, a very good agreement between the two datasets can be found for both months. In comparison to the GOME LER–MERIS BSA plots, the scatter is remarkably reduced and no clusters of large differences are detectable. Further, most values are almost perfectly aligned along the bisecting line. The few higher MERIS albedo values for MODIS BSA between approximately 0.15 and 0.3

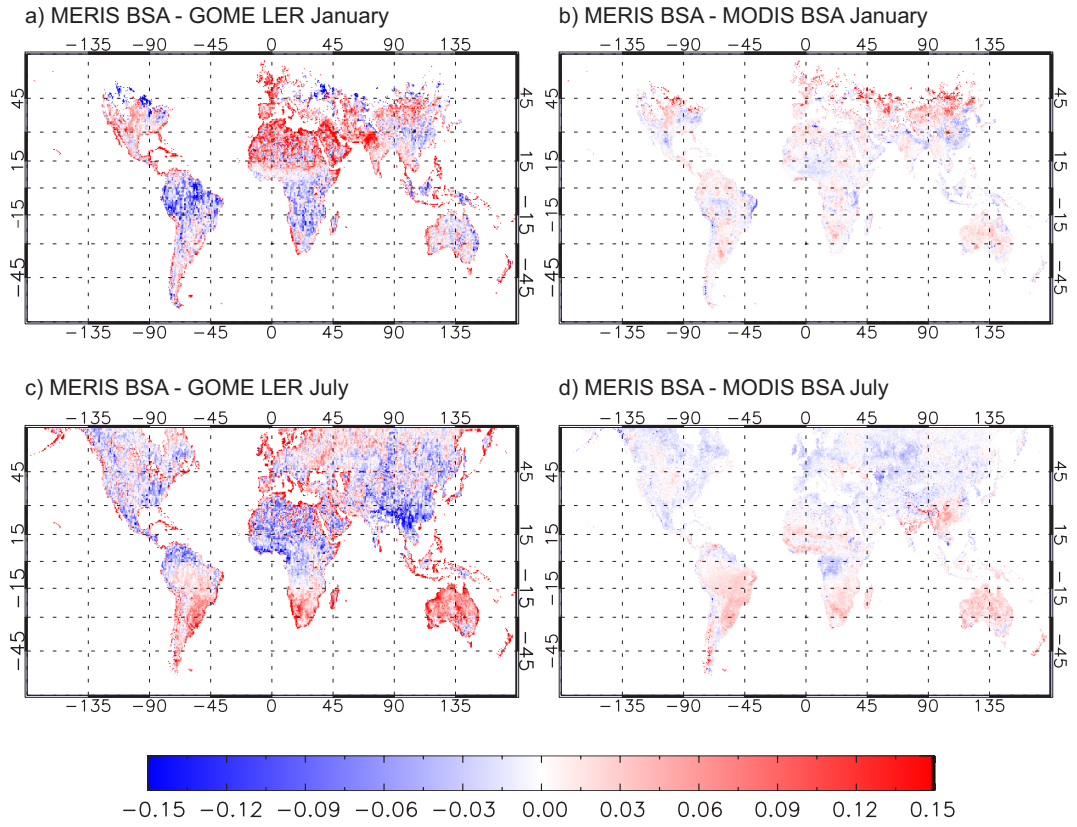

Fig. 4. Difference maps of MERIS BSA–GOME LER (754 nm and 758 nm) and MERIS BSA–MODIS BSA (865 nm and 858 nm) for January and July, respectively.

can mainly be assigned to pixels adjacent to snow covered areas, for example in the boreal forest of northern latitudes in January or in the Andes during July (cf. Fig. 4).

Table 1 summarizes selected statistical parameters from the comparison between the MERIS BSA, MODIS BSA, and GOME LER. In order to reduce the impact of outliers (mostly residual snow) 5% of all match-ups with the largest absolute difference are discarded from the calculation (but shown in the scatter density plot in Fig. 3). These statistics underline the findings from Fig. 3 discussed above. MERIS BSA compares better to MODIS BSA than to the GOME LER dataset. The correlation coefficient obtained for the comparison between MERIS and MODIS is 0.98 for the entire dataset and 0.98 and 0.97 for January and July, respectively. Comparing MERIS BSA to GOME LER results in correlation coefficients of ∼0.8. In addition, the linear regression coefficients reveal almost no offsets and slopes near unity for the MERIS BSA–MODIS BSA comparison. In contrary, usually relatively large offsets and slopes considerably smaller than one are found for the MERIS BSA–GOME LER comparison reflecting the large underestimation and mismatch along coastlines in the GOME LER dataset. It is also noteworthy that the average differences between the three datasets are in general clearly below 0.01, except for the MERIS channel at 775 nm and GOME channel at 772 nm which are slightly higher than 0.01. The average differences for the MERIS BSA–MODIS BSA comparison are below 1% of the average (snow excluded) MERIS BSA of the entire year (∼0.28 at 858 nm). Further, the σ of the differences from the MERIS BSA–MODIS BSA comparisons are approximately three times smaller than from the MERIS BSA–GOME LER comparison. We calculated statistical parameters for all individual months of the year. With regard to the MERIS BSA–MODIS BSA comparison, this does not result in a seasonal pattern for any parameter. The smallest correlation coefficient is 0.97 for June and July, the largest average difference is about 0.002 for September. We conclude that the MERIS BSA database compares well and considerably better than GOME LER to MODIS BSA.

Although not the primary objective of this study, we also evaluated the MERIS database in the visible wavelength region because of its potential application for the retrieval of NO_2 tropospheric column amount. The MERIS albedo values from 442 nm and 490 nm are interpolated to the corresponding MODIS spectral band at 470 nm. The entire twelve month data base of MERIS BSA is, like in the NIR analysis, in better agreement to MODIS than the GOME LER with a correlation coefficient of 0.97 (0.80 for GOME LER) and

Table 1. Comparison between GOME LER, MERIS BSA, and MODIS BSA for snow-free pixels for the entire globe.

		R^1	average difference	σ^2	offset	slope
Whole Year	GOME 758 nm–MERIS 754 nm	0.80	−0.002	0.057	0.067	0.730
	GOME 772 nm–MERIS 775 nm	0.81	−0.013	0.057	0.078	0.733
	MODIS 858 nm–MERIS 865 nm	0.98	0.000	0.017	−0.001	1.005
January	GOME 758 nm–MERIS 754 nm	0.79	−0.005	0.063	0.057	0.792
	GOME 772 nm–MERIS 775 nm	0.80	−0.016	0.062	0.068	0.795
	MODIS 858 nm–MERIS 865 nm	0.98	−0.002	0.018	0.001	1.002
July	GOME 758 nm–MERIS 754 nm	0.79	−0.002	0.056	0.092	0.637
	GOME 772 nm–MERIS 775 nm	0.79	−0.014	0.056	0.103	0.642
	MODIS 858 nm–MERIS 865 nm	0.97	−0.001	0.016	0.005	0.984

[1] R: correlation coefficient.

[2] σ: standard deviation of differences.

an average difference of 0.003 (−0.013 for GOME LER). Zhou et al. (2010) compared GOME/TOMS LER (440 nm) and the MODIS reflectance products at 470 nm over Europe with similar findings. Integrating the MODIS products in the NO_2 retrieval subsequently resulted in NO_2 tropospheric column amounts up to 15% higher in summer and 20%–60% higher in winter.

4.1.4 Spatial differences

The findings from the statistical analysis are underlined in the spatial differences shown in Fig. 4. The differences between MERIS BSA and MODIS BSA near 860 nm are generally much lower than the ones between MERIS BSA and GOME LER near 760 nm. The largest discrepancies to MODIS are found in regions affected by (subgrid) snow cover persistent in the MERIS BSA dataset, e.g. near the boreal forests in January or the Himalaya and southern Andes during July. The MERIS BSA is presumably more affected by snow contamination because the MODIS BSA is in principle based on a larger amount of individual observations which allows a better exclusion (and consequent filling) of snow affected surfaces. For example, MODIS (on-board Terra and Aqua) obtains near daily global coverage whereas MERIS requires three days to achieve global coverage. Furthermore, MODIS is based on a five years aggregate instead of four years for MERIS. Snow cover differences between the periods January 2000 to January 2004 (MODIS aggregate) and November 2002 to November 2006 (MERIS aggregate) might also introduce some small discrepancies between the two datasets. In addition, MERIS reveals slightly higher albedo values in Eastern South America, Southern Africa, East Asia, and Australia in July. Somewhat higher MODIS albedo values can be observed in central Africa and some regions in northern latitudes higher than 45°. Jin et al. (2003) speculated that probably intense biomass burning in the Amazon basin as well as land cover change can lead to differences when comparing albedo products over eastern South America. Apart from arid areas, the previously mentioned regions with deviating albedo values usually provide a very low number of high quality retrievals for the MODIS albedo and BRDF products due to persistent cloud coverage (tropics) or seasonal snow and cloud contamination (Gao et al., 2005; Moody et al., 2005). Some differences thus also appear because MODIS BSA uses a temporal interpolation technique but in the MERIS BSA database the value from the closest month is assigned to missing grid cells. Finally, in the Saharan desert and the Arabian peninsula, MERIS BSA and MODIS BSA are in very good agreement.

The coastline mismatch of the GOME database is pronounced in most areas of the world and for both months illustrated in Fig. 4, with the exception of tropical Africa, South America in winter and East Asia in summer. MERIS and GOME also reveal some large differences in arid regions, e.g. in the Saharan desert and the Arabian Peninsula in January or Australia and the Namib desert in July. Negative differences (GOME >MERIS, given in blue) in the tropics are likely due to an overestimation of GOME LER caused by residual cloud coverage near the Intertropical Convergence Zone (ITCZ), e.g. in South America, west coast of Africa or Asia (Koelemeijer et al., 2003). This difference follows the northward migration of the ITCZ from January to July. While MERIS BSA shows higher values than GOME for the Sahara and the Arabian peninsula in January, for many pixels the opposite is the case for July. Desert regions are challenging for surface albedo retrieval because of the presence of mineral dust and the usually high albedo of the surface. Dust aerosols can lower the measured reflectance at the TOA through absorption (Kaufman et al., 2001) so the minimum LER used to compile the GOME LER climatology does not correspond to the aerosol-free observation anymore. Although Fournier et al. (2006) corrected for this

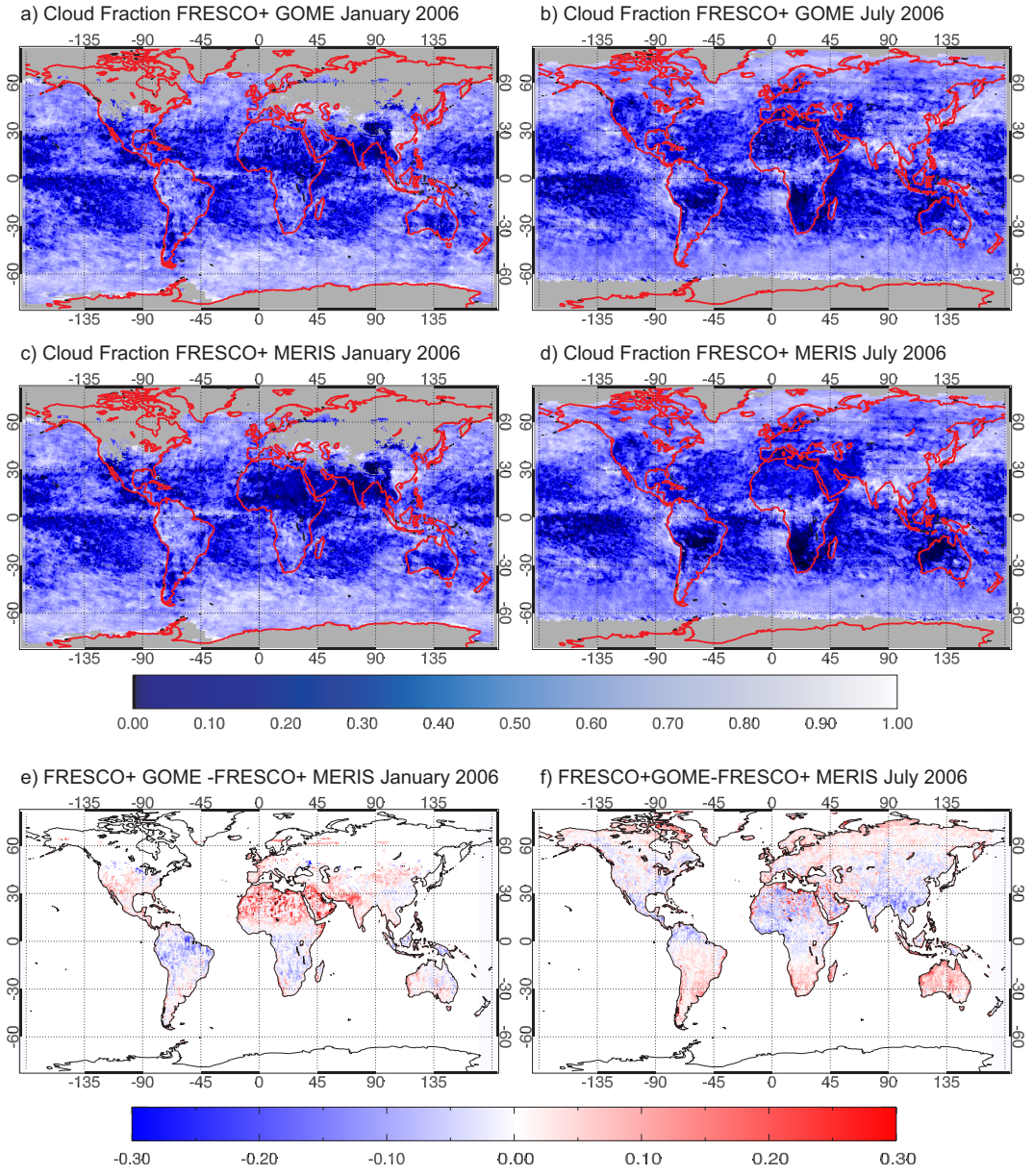

Fig. 5. Monthly mean FRESCO+ GOME and FRESCO+ MERIS effective cloud fraction **(a–d)** as well as their absolute differences **(e–f)** for January and July 2006. Note that ocean pixels are processed with the GOME LER data also in the MERIS retrieval so that no differences occur over water. Grid cells with no valid retrieval, e.g. due to permanent snow coverage are given in a grey color.

effect, the deviations between GOME and MERIS are still large when considering the good agreement between MERIS and MODIS. However, the MERIS and MODIS albedo products might be also strongly affectedby the presence of desert dust aerosols. Both products rely on the aerosol optical depth (AOD) retrieval over land from MODIS (Kaufman and Tanré, 1998) which does not provide AOD over bright surfaces like snow or desert (Remer et al., 2008). Therefore, aerosol parameters from predefined climatologies (cf., Vermote et al., 1997; Koepke et al., 1997) are used to derive surface reflectance in this case.

4.2 FRESCO+ results using MERIS albedo

4.2.1 Comparison to results from the GOME database

The effect of the MERIS albedo climatology on O_2 A-band cloud retrieval is demonstrated using two exemplary months of SCIAMACHY data (January and July 2006). Global maps of monthly averaged effective cloud fraction obtained with the GOME LER and MERIS BSA datasets as well as their differences are depicted in Fig. 5. The global cloud patterns are clearly detectable in both FRESCO+ results, e.g. higher

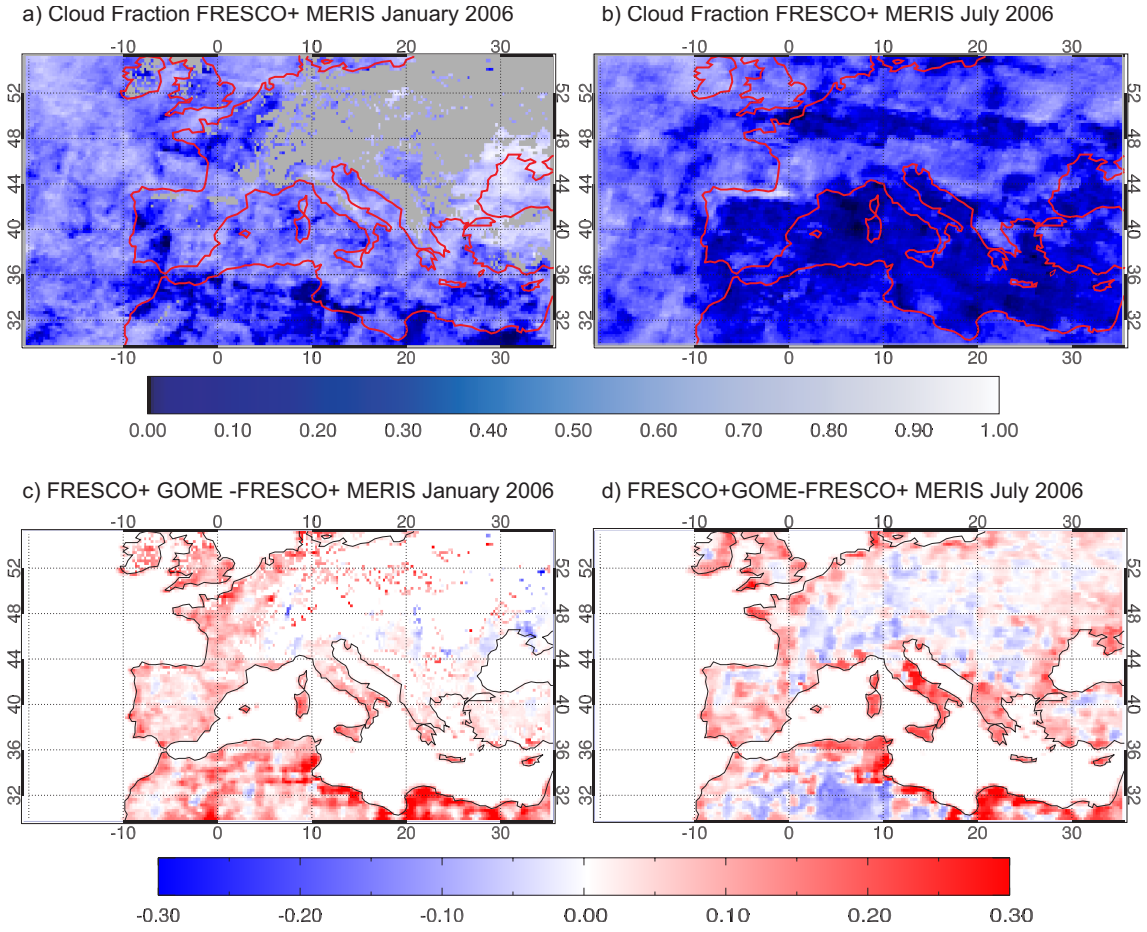

Fig. 6. Monthly mean FRESCO+ MERIS effective cloud fraction **(a–b)** as well as the absolute differences **(c–d)** to FRESCO+ GOME over Europe for January and July 2006. Note that ocean pixels are processed with the GOME LER data also in the MERIS retrieval so that no differences occur over water. Grid cells with no valid retrieval, e.g. due to permanent snow coverage are given in a grey color.

cloud fractions in the tropics and at higher latitudes or the northward movement of the ITCZ in summer. As FRESCO+ retrieves an effective cloud fraction (radiometric equivalent fraction of a thick cloud with A_c of 0.8, c.f. Sect.2) the global maps do not represent the geometrical cloud fractions which are usually higher. For instance, c irrus clouds with a relatively low optical thickness are compensated in the FRESCO+ algorithm by reducing the effective cloud fraction. Such an effect would probably not be apparent in geometrical cloud fractions, especially when retrieved from sensors with a high spatial resolution (e.g. MODIS). Differences generally follow the trend identified in Fig. 4 and discussed in the previous section. For example, the higher MERIS BSA over Western Australia results in much smaller effective cloud fractions in July. The relatively higher MERIS BSA over the Sahara and the Arabian peninsula in January leads to lower effective cloud fractions in these regions which is not the case for July. Increased aerosol abundance and absorption during summer might lead to an underestimation of surface albedo in arid regions and therefore an overestimation of cloud fraction. However, the MERIS BSA dataset results in a distinct smoother distribution of effective cloud fractions over these arid regions (also in July). We attribute this effect to the better spatial resolution of the MERIS BSA database that allows a better representation of the quite heterogeneously distributed soils and rock types in the Saharan desert (cf. Tsvetsinskaya et al., 2002).

A more detailed view is given in Fig. 6 for a subset covering Europe and parts of North Africa. The effect of the MERIS climatology is clearly detectable for both months. Mediterranean islands like Corsica or Sicily have a strong impact on the water-land mismatch in the GOME LER dataset (cf. Fig. 1) leading to an overestimation of effective cloud fraction. Mediterranean islands are not captured well by the GOME LER climatology in general. The increased effective cloud fractions along the northern African coast in the FRESCO+ GOME results are another example of the mismatch along coastlines. An improved effective cloud fraction retrieval from FRESCO+ in coastal areas is desirable considering that a majority of the world's largest megacities are located in the immediate vicinity to the ocean. Several studies underlined the scientific interest of air pollution assessments

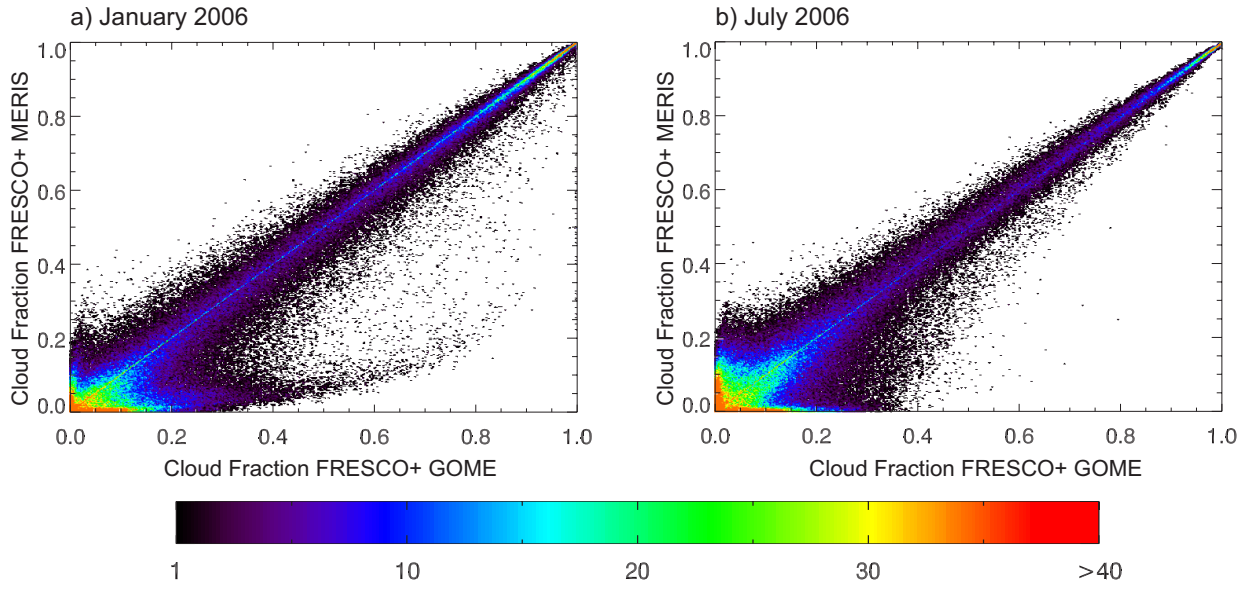

Fig. 7. Scatter density plots of FRESCO+ MERIS effective cloud fraction as a function of FRESCO+ GOME effective cloud fraction for January (left) and July 2006 (right). Only snow/ice-free values over land are compared.

in these areas from spaceborne trace gas retrievals (e.g., Richter et al., 2005; van der A et al., 2008).

Scatter density plots of the cloud fractions obtained from the MERIS BSA data base as a function of the ones obtained from the GOME LER database are illustrated in Fig. 7 for January and July 2006. In order to reduce the influence of snow contamination exclusively values obtained between 50° S and 50° N are plotted. The majority of points is aligned close to the bisecting line. The bimodal distribution of cloud fractions is mirrored by an increased number of very low and very high values. The largest differences are mostly observable for effective cloud fractions lower than ∼0.3. This on the one hand underlines that the impact of surface albedo is largest for small effective cloud fractions and on the other hand is of particular interest for trace gas retrievals which are restricted to relatively small cloud fractions (usually < 0.3). The effect of the higher surface reflectivity of arid regions (cf. Fig. 5) and the enhanced spectral contrast along coastlines (cf. Fig. 6) can be detected in Fig. 7 where the FRESCO+ GOME results reveal more enhanced effective cloud fractions for low values of the MERIS results than contrariwise. The feature of relatively low MERIS BSA cloud fractions for GOME LER cloud fractions higher than 0.3 in the January scatter density plot (Fig. 7a) can mainly be ascribed to the above-mentioned geographical areas, i.e. coastlines, deserts and occasionally to snow cover affected areas in northern latitudes. The correlation coefficients are high (0.94 for January and 0.96 for July), the offsets low (−0.008 for January and 0.000 for July) and the slopes almost unity (1.002 for January and 1.000 for July). However, the results based on MERIS BSA reveal lower mean cloud fraction for global snow/ice-free land surfaces between 50° S and 50° N, e.g. 0.30 vs. 0.34 for GOME LER for January and 0.24 vs. 0.26 for the month of July 2006 which underlines the general reduction of the artefacts mentioned above.

With regard to cloud pressure, use of the MERIS database leads to similar results as the GOME LER. We consider exclusively cloud pressure for effective cloud fractions $\geq$0.1 (in accordance to Wang et al., 2008). The MERIS BSA results reveal slightly lower average cloud pressure for January 2006 (GOME: 677.4 hPa, MERIS: 666.9 hPa; difference: 10.5 hPa ± 58.1 hPa) and almost identical average cloud pressure for July 2006 (GOME: 684.4 hPa, MERIS: 683.9 hPa; difference: 0.5 hPa ± 48.1 hPa). In addition, the correlation coefficients between the two sets are very high (0.96 for January 2006 and 0.97 for July 2006). Koelemeijer et al. (2002) showed that cloud pressure is not very sensitive to changes in surface albedo. The reason is that cloud pressure is derived from the depth of the O_2 A-band and since O_2 is a strong absorber in this band, most of the light is absorbed before reaching the surface such that the reflected light from the surface has only a small impact on the retrieval.

4.2.2 Comparison to HICRU

The Heidelberg iterative cloud retrieval (HICRU, Grzegorski et al., 2006) provides effective cloud fraction and cloud top pressure from SCIAMACHY data and is used herein to evaluate the impact of the new albedo climatology on the FRESCO+ retrievals. HICRU is especially suitable for this purpose as it is based on the same concept of effective cloud fraction in contrast to other available cloud parameters from

other algorithms (e.g. Kokhanovsky et al., 2009). In contrast to FRESCO+, HICRU takes advantage of the higher spatial resolution of the Polarisation Measurement Devices (PMD, $7 \times 30\,\mathrm{km}^2$ across/along track) to derive cloud fraction. For each scene, HICRU first defines an upper intensity threshold representing fully cloudy SCIAMACHY pixels (I_{cloudy}) and a lower intensity threshold standing for the intensity of cloud free pixels ($I_{\mathrm{cloudfree}}$). The effective cloud fraction is subsequently found by linear interpolation, i.e. by dividing the difference between the measured intensity and $I_{\mathrm{cloudfree}}$ by $I_{\mathrm{cloudy}}-I_{\mathrm{cloudfree}}$. The lower intensity threshold is a priori determined by iterative image sequence analysis of PMD3 (617–705 nm) intensities and is a function of longitude, latitude, and surface albedo. $I_{\mathrm{cloudfree}}$ is mapped to a grid with a spatial resolution (latitude × longitude) of $0.1° \times 0.062°$. The upper threshold is found by radiative transfer calculations and as a function of solar zenith and view zenith angles. A detailed description of the methodology can be found in Grzegorski et al. (2006) and Grzegorski (2009). The accuracy of the effective cloud fraction obviously depends on the two thresholds. HICRU fails in the presence of snow and ice because these surfaces are often brighter than clouds with high albedo.

Grzegorski et al. (2006) compared HICRU to FRESCO (for latitudes between 50° N and 50° S to avoid snow contamination) and found slightly better correlations over ocean than over land. In this study we exclusively compare results over land as the MERIS albedo data does not provide values over ocean. FRESCO+ reports effective cloud fraction corresponding to a Lambertian cloud albedo of 0.8 and HICRU derives I_{cloudy} as a function of the observation geometry with a fixed optical thickness of 50 and the assumption of a scattering cloud with a vertical extension of 1 km which approximately corresponds to a Lambertian cloud with an albedo of 0.9. In order to account for these different assumptions and for better comparability, we convert the FRESCO+ effective cloud fractions such that they correspond to a Lambertian cloud albedo of 0.9. An empirical relation (third order polynomial fit) between the ratio of the effective cloud fraction for a cloud albedo of 0.9 and 0.8 as a function of surface albedo has been established by running FRESCO+ for one SCIAMACHY orbit (4 February 2007, 10:30 UTC) for the two cloud albedo values (Fig. 8). Cloud fractions are henceforth restricted to values below 0.8 because retrieved effective cloud fractions larger than one are set to 1.0 in the original FRESCO+ retrieval leading to an upper limit of approximately 0.9 after the conversion.

Figure 9 demonstrates that the FRESCO+ MERIS results are in better agreement to the HICRU effective cloud fractions for both months than FRESCO+ GOME. Especially the overestimation of small cloud fractions where the impact of the surface reflectivity is large as well as the scatter are clearly reduced. The averaged FRESCO+−HICRU difference decreases from 0.02 (0.03) to 0.00 (0.02) and the correlation increases from 0.93 (0.92) to 0.96 (0.96) for January

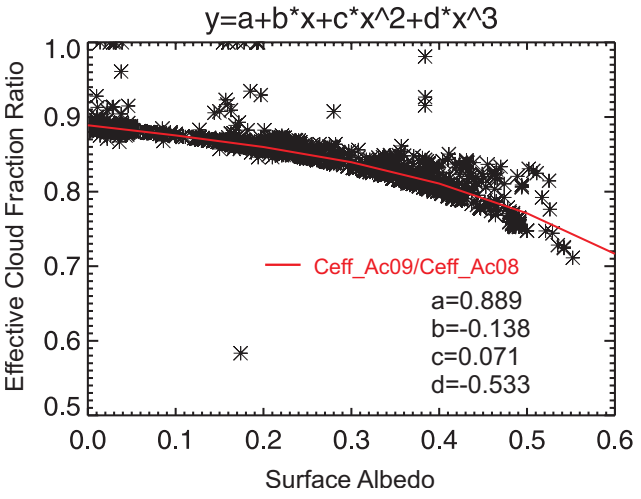

Fig. 8. Ratio of FRESCO+ effective cloud fractions for an assumed cloud albedo of 0.9 and 0.8, respectively. Based on FRESCO+ retrievals from one SCIAMACHY orbit (4 February 2007, 10:30 UTC).

(and July, cf. Table 2). FRESCO+ effective cloud fractions lower than 0.075 for HICRU cloud fractions larger than 0.225 in the January plots can be assigned to residual snow signals mostly in the MERIS BSA climatology. However, overall less than 0.3% of all retrievals are affected, mostly in Canada (∼90° W, >40° N) and Siberia (∼100° E, >40° N, cf. Fig. 10).

Distinct improvements for FRESCO+ MERIS are achieved for a subregion covering the Sahara desert and Arabian peninsula [15° N–30° N, 15° W–60° E] for January 2006. The correlation coefficient increases from 0.75 to 0.92, the RMSE decreases from 0.13 to 0.05, and the averaged difference decreases from 0.08 to 0.01 (Table 2). In contrast, although the σ (from 0.08 to 0.05), RMSE (from 0.12 to 0.09), and correlation (from 0.62 to 0.76) improves, the averaged difference remains constant for July (Table 2). The MERIS and MODIS black-sky albedo are in very good agreement in this region throughout the year (e.g. in July $R = 0.99$, offset = −0.01, slope = 1.02, difference of mean = 0.00). The better correlation, σ, and RMSE can be explained through the enhanced spatial resolution of the MERIS database which better captures the heterogeneous surface features in the desert. As noted in Muller (2008) absorbing aerosols seriously hamper an accurate albedo retrieval. The study of de Graaf et al. (2005) revealed that the annual occurrence of desert dust is highest in the summer months which indicates that both, MERIS and MODIS black-sky albedo, are underestimated for this time of the year. In addition, FRESCO+ effective cloud fractions are very sensitive to small changes of surface albedo values, especially over highly reflective targets. The following estimate of the change in effective cloud fraction due to changes in surface albedo is given in Koelemeijer et al. (2002):

Table 2. Comparison between FRESCO+ GOME/MERIS and HICRU cloud fraction over snow/ice-free land surfaces between 50° N and 50° S as well as over a subscene containing the Saharan desert and the Arabian peninsula [15° N–30° N and 15° W–60° E]. In FRESCO+, a cloud albedo of 0.9 is used and only cloud fractions < 0.8 are considered.

		$\overline{\text{FRESCO+}-\text{HICRU}}$[1]	N[2]	R[3]	σ[4]	offset	slope	RMSE[5]
			Global					
January	FRESCO+ GOME	0.02	124 455	0.93	0.06	0.02	0.96	0.08
	FRESCO+ MERIS	0.00	124 455	0.96	0.04	0.00	0.99	0.05
July	FRESCO+ GOME	0.03	154 663	0.92	0.06	0.03	0.99	0.08
	FRESCO+ MERIS	0.02	154 663	0.96	0.04	0.01	1.04	0.06
			Saharan desert and Arabian peninsula					
January	FRESCO+ GOME	0.08	14 203	0.75	0.09	0.06	0.93	0.13
	FRESCO+ MERIS	0.01	14 203	0.92	0.03	0.02	0.81	0.05
July	FRESCO+ GOME	0.07	15 540	0.62	0.08	0.04	1.05	0.12
	FRESCO+ MERIS	0.07	15 540	0.76	0.05	0.07	0.92	0.09

[1] $\overline{\text{FRESCO+}-\text{HICRU}}$: average difference between FRESCO+ and HICRU.

[2] N: number of match-ups.

[3] R: correlation coefficient.

[4] σ: standard deviation of FRESCO+−HICRU.

[5] RMSE: root mean square error.

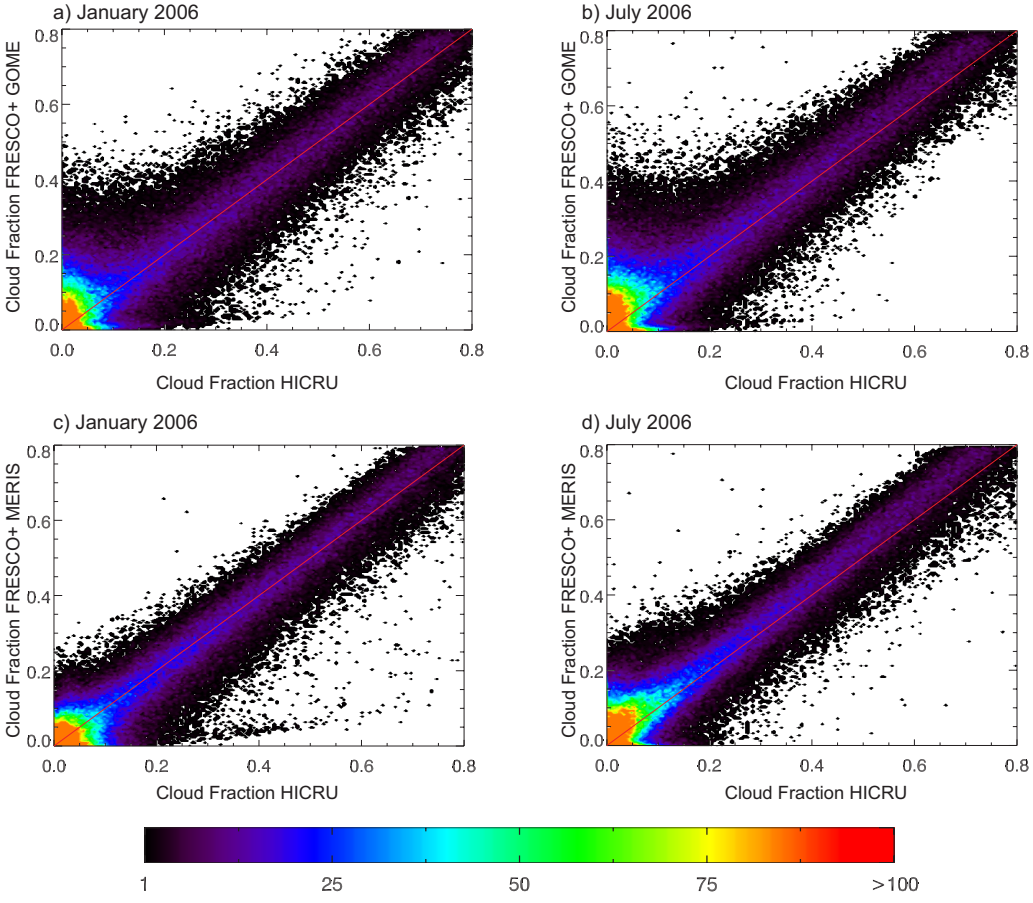

Fig. 9. FRESCO+ effective cloud fractions (upper panels with GOME LER, lower panels with MERIS BSA) as a function of HICRU cloud fractions for latitudes between 50° N and 50° S and snow/ice-free observations and for January (left) and July 2006 (right), respectively. FRESCO+ effective cloud fractions are converted to a cloud albedo of 0.9 and only cloud fractions < 0.8 are considered (see text).

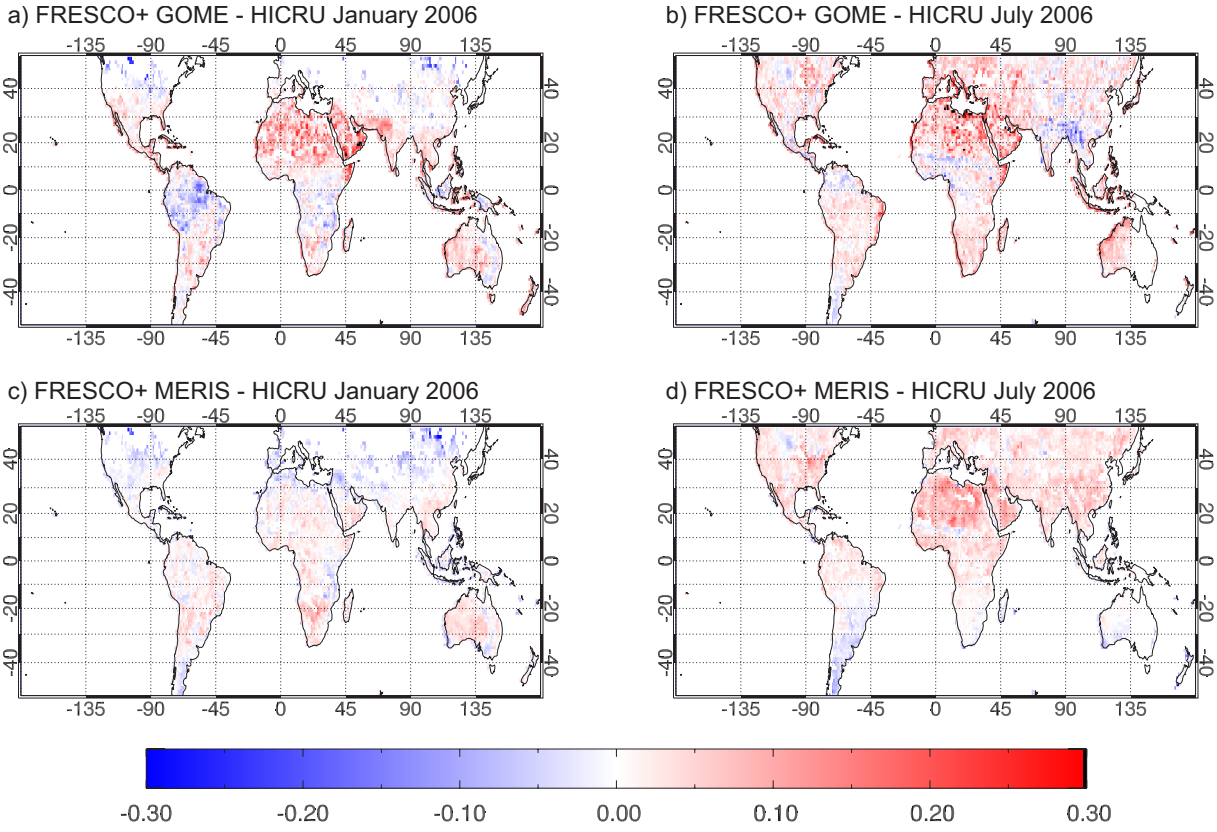

Fig. 10. Difference maps of monthly averaged effective cloud fractions per 1° × 1° grid box between FRESCO+ (GOME (upper plots) and MERIS (lower plots)) and HICRU cloud fractions for January and July 2006. FRESCO+ effective cloud fractions are converted to a cloud albedo of 0.9 and only cloud fractions <0.8 are considered (see text).

$$\Delta c = -\frac{1-c}{A_c - A_s}\Delta A_s \quad (2)$$

HICRU reveals an average effective cloud fraction (c) of 0.037 for July 2006 over the Saharan desert and Arabian peninsula (cf. Table 2), the mean A_s of MERIS in this area is 0.394, A_c of FRESCO+ is 0.9, and Δc is 0.07 (see Table 2). Thus, disregarding all other error sources and assuming HICRU provides the true cloud fraction, Eq. (2) suggests that MERIS BSA is underestimated by 0.035 (∼9.0%) in July in the considered area.

Figure 10 presents global maps of the difference between FRESCO+ MERIS or GOME to HICRU. Again, FRESCO+ MERIS−HICRU reveals a smoother geographical distribution in comparison to FRESCO+ GOME−HICRU due to the better spatial resolution of the MERIS BSA database. Both FRESCO+ retrievals occasionally underestimate effective cloud fraction in regions adjacent to snow covered areas, i.e. in the boreal forests in the northern hemisphere in January 2006. For January 2006, the obtained enhancements are particularly detectable over the above-mentioned arid regions but also over large parts of the Americas. FRESCO+ GOME underestimates effective cloud fractions in the ITCZ in both months, e.g. in Northern South America due to residual cloud signatures in the GOME LER data base (Koelemeijer et al., 2003, cf. Fig. 4, Sect. 4.1.4). Taken together, we conclude that FRESCO+ MERIS is in clearly better agreement to HICRU than FRESCO+ GOME.

4.2.3 Impact on trace gas retrievals

Surface albedo affects trace gas retrievals directly through the radiative transfer computations of the clear-sky air mass factor in the fitting window of the trace gas and indirectly via cloud parameter retrievals. With regard to the direct effect, an increase in surface albedo increases the air mass factor thereby decreasing the vertical column density. The study of Boersma et al. (2004) reported a 5% change for clean cases and 8% change for polluted cases in NO_2 tropospheric vertical column densities (NO_2 VCD_{trop}) for a surface albedo change of 0.02 at 440 nm. In Sect. 4.1.3 we found the MERIS BSA climatology to be ∼0.01 lower than GOME LER at 470 nm so we expect the direct impact of the MERIS database to be on average a small increase in NO_2 VCD_{trop} of 2 to 4%. However, a more in-depth analysis of the first effect of the MERIS BSA climatology is beyond the scope of this work and therefore left for future studies.

In order to assess the indirect impact, we processed SCIAMACHY NO_2 VCD_{trop} over Europe and North Africa [28° to 55° N, −10° to 30° E] for July 2006 with the FRESCO+ GOME and FRESCO+ MERIS cloud parameters, respectively. The a priori profiles were taken from the Model for Ozone and Related Chemical Tracers, version 4 (MOZART-4, Emmons et al., 2010) and the radiative transfer code LIDORT (Spurr, 2008) was used for air mass factor calculations. The tropospheric air mass factor was computed as a combination of the clear-sky and cloudy-sky air mass factor following the independent pixel approximation. For a detailed description on NO_2 VCD_{trop} retrievals, the reader is referred to the literature (e.g. Boersma et al., 2004; Zhou et al., 2010). The impact of a change of the effective cloud fraction on NO_2 VCD_{trop} is depicted in Fig. 11a for all coincident FRESCO+ GOME and FRESCO+ MERIS results with an effective cloud fraction lower than 0.3. In general, an increase of cloud fraction due to a decreased surface albedo enhances the tropospheric air mass factor and hence decreases NO_2 VCD_{trop} (and vice versa) when the cloud is inside or below the trace gas layer. On the other side, an increase of cloud fraction may reduce the tropospheric air mass factor when the cloud is located well above the trace gas layer because high clouds shield tropospheric NO_2 from detection. The average cloud pressure from FRESCO+ in July 2006 is ∼870 hPa indicating that the majority of the clouds in this analysis is low. The linear regression from the points plotted in Fig. 11a denotes that a decrease of the effective cloud fraction of 0.05 leads to an increase of 5.4% in NO_2 VCD_{trop} (slope = -108.08 ± 1.9). However, there is considerable scatter in the results due to variations in cloud pressures (and therefore also variations in the ghost columns) and the level of pollution. The impact is generally stronger in polluted regions and weaker in clean areas. The density distribution indicates a slight shift toward higher effective cloud fractions for FRESCO+ MERIS because overestimated FRESCO+ GOME cloud fractions do frequently not pass the threshold of 0.3 when FRESCO+ MERIS cloud fractions do.

The spatial distribution of monthly averaged NO_2 VCD_{trop} derived with the FRESCO+ MERIS cloud parameters for July 2006 is presented in Fig. 11b. The average change of cloud fraction for the region mapped in Fig. 11b and 11c is 0.025 and the cloud pressure increases by 19 hPa which overall leads to a slight decrease of NO_2 VCD_{trop} of only around 0.01×10^{15} [molec cm^{-2}] or about 0.5%. However, the differences can be quite large on a regional scale (Fig. 11c). For example, the absolute differences are obviously larger in polluted regions (c.f. Fig. 11b) like England, the Netherlands, or the Ruhr region in Germany where NO_2 VCD_{trop} can change by more than 1×10^{15} [molec cm^{-2}]. The most distinct exception can be found in the northern part of England (north of 53° N) where NO_2 VCD_{trop} increases about 0.6×10^{15} [molec cm^{-2}] (6%), although the effective cloud fraction decreases (∼0.05), which is most likely caused by the decrease of cloud pressure from ∼770 hPa to ∼540 hPa.

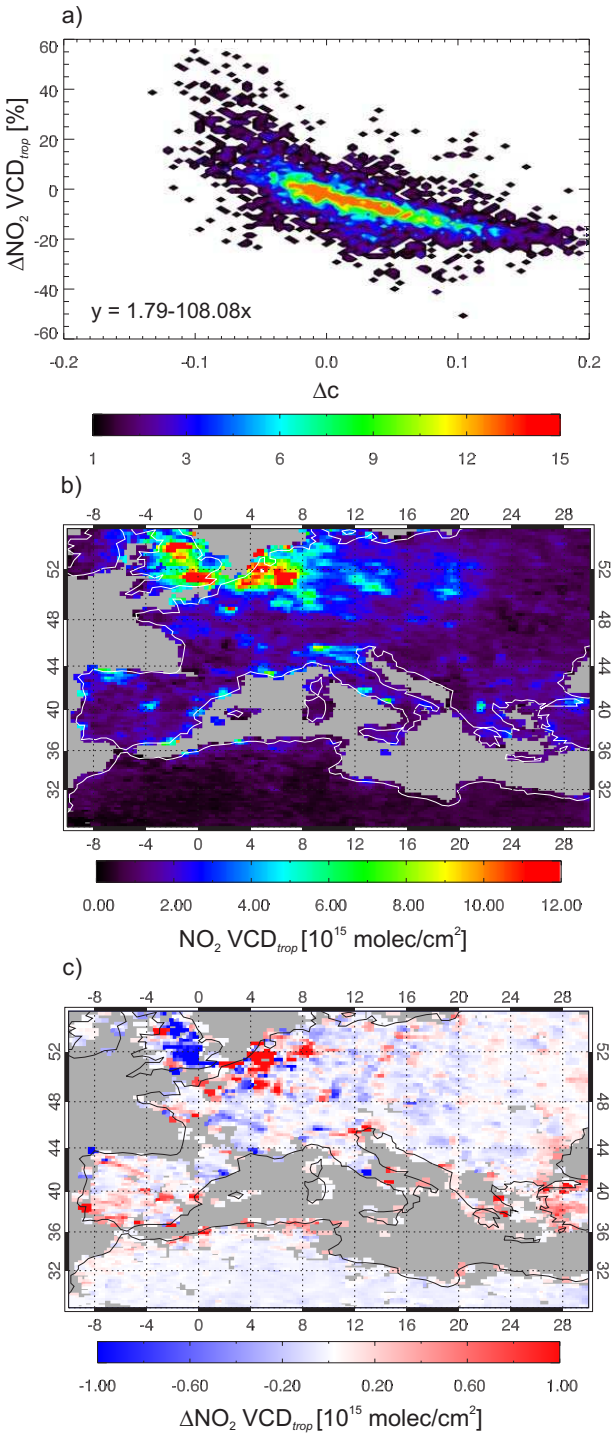

Fig. 11. a) Scatter density plot of the change of SCIAMACHY derived NO_2 tropospheric vertical column density (NO_2 VCD_{trop}) due to a change of the effective cloud fraction (FRESCO+ MERIS - FRESCO+ GOME). b) Spatial distribution of NO_2 VCD_{trop} derived with the FRESCO+ MERIS cloud parameters over Europe for July 2006. c) Difference of the NO_2 VCD_{trop} distribution between the retrievals with FRESCO+ MERIS and FRESCO+ GOME cloud parameters.

Although the effective cloud fraction changes quite strongly in North Africa (c.f. Fig. 6d), almost no changes appear in this region because the NO_2 VCD_{trop} is low. The improvements obtained when integrating the MERIS climatology in FRESCO+ can also be observed along coastlines, e.g. around the Mediterranean coast where the reduced cloud fractions of FRESCO+ MERIS along coastlines lead to higher NO_2 VCD_{trop}. No differences are obtained for southern Italy and some Mediterranean islands because FRESCO+ GOME effective cloud fractions exceed the threshold of 0.3 due to the strong underestimation of surface albedo in the GOME LER data. In contrast, applying the MERIS dataset to FRESCO+ leads to valid NO_2 VCD_{trop} in these areas (Fig. 11b).

FRESCO+ cloud parameters can also be used for trace gas retrievals in the UV spectral range (such as O_3, SO_2, HCHO, or BrO). For this reason, we compare TOGOMI (Total Ozone algorithm for GOME using the OMI algorithm, Valks and van Oss, 2003) total O_3 columns of version 1.3 processed with the FRESCO+ GOME and version 2.0 processed with the FRESCO+ MERIS cloud parameters, respectively. The change of total O_3 as a function of the change of effective cloud fraction is illustrated in Fig. 12a over land for the above mentioned study region. Here no threshold on the effective cloud fractions is applied for the O_3 analysis. In general, the impact of the MERIS dataset is similar to the one discussed above for the NO_2 VCD_{trop}. O_3 VCD decreases with increasing cloud fraction and this change depends on the total trace gas column. The linear regression from the points plotted in Fig. 12a indicates that a change of the effective cloud fraction of 0.05 leads to a change of 0.65% in the O_3 total column (slope $= -12.97 \pm 0.05$). The average effective cloud fraction for July 2006 slightly decreases by -0.007 which leads to an increase of O_3 VCD of 0.5 DU (0.17%). Again, regional deviations between the two TOGOMI versions can be distinctively larger. For example, along the coastlines total O_3 columns can increase in the range 5–10 DU ($\sim$1.6–3.2%, Fig. 12b). Valks and van Oss (2003) reported a total error of TOGOMI O_3 VCD between 2.5% (clear pixel) and 3.3% (completely cloudy pixel) which underlines that the MERIS dataset has a clear impact on trace gas retrievals on regional scale. Finally, in regions where MERIS BSA is lower than GOME LER and cloud fractions are therefore higher (e.g. North Africa or parts of France) O_3 VCD decreases. In general, the O_3 difference map in Fig. 12b reveals the same features as the effective cloud fraction difference map in Fig. 6d. Altogether, these preliminary results of NO_2 VCD_{trop} and O_3 VCD derived with FRESCO+ MERIS suggest that the presented MERIS BSA climatology has a pronounced and beneficial effect on trace gas retrievals on regional scale even if the average differences are small.

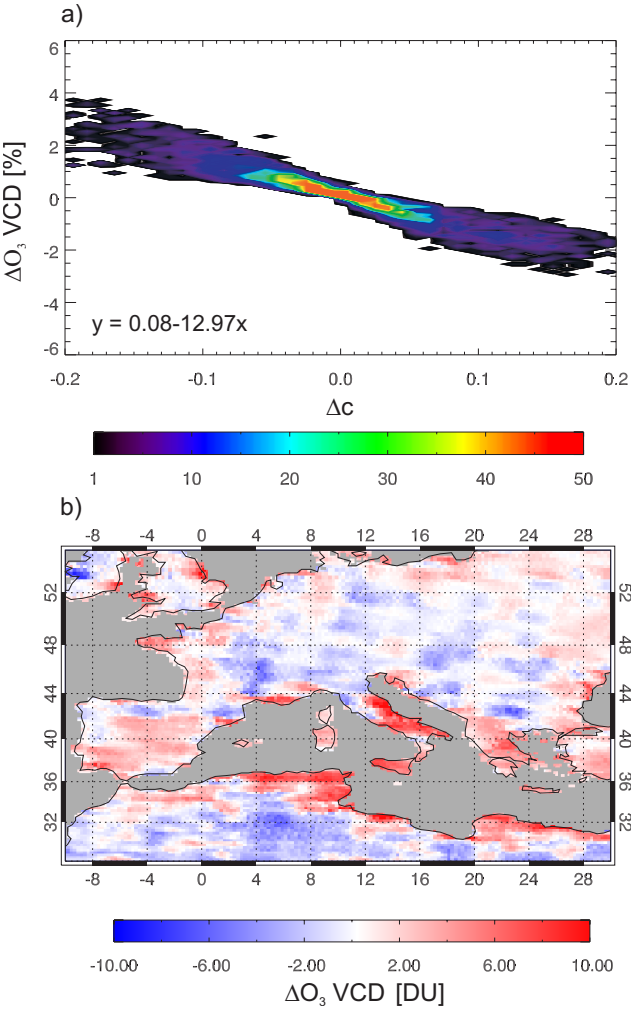

Fig. 12. a) Scatter density plot of the change of GOME derived total O_3 VCD due to a change of the effective cloud fraction (FRESCO+ MERIS - FRESCO+ GOME) over Europe and North Africa for July 2006. b) Map of differences between TOGOMI version 2.0 (processed with FRESCO+ MERIS) and TOGOMI version 1.3 (processed with FRESCO+ GOME). Positive values indicate higher effective cloud fractions for FRESCO+ MERIS and higher O_3 VCD for TOGOMI version 2.0.

5 Conclusions

A new albedo climatology created from MERIS Albedomap data with the aim to enhance the operational retrieval of effective cloud fraction over land surfaces in the O_2 A-band was introduced. We tested the substitution of the $1° \times 1°$ GOME LER climatology in the FRESCO+ cloud retrieval with this MERIS black-sky albedo dataset on a grid of $0.25° \times 0.25°$. Further, the MERIS climatology was compared to MODIS black-sky albedo and to the GOME LER database. In order to assess the obtained improvements, FRESCO+ was run for two exemplary months of SCIAMACHY data (January and July 2006) and the results were

related to retrievals from the cloud retrieval algorithm HICRU. Finally, the indirect effect of the presented albedo climatology on spaceborne NO_2 VCD_{trop} and O_3 VCD retrievals was evaluated. The main findings can be summarized as follows:

1. The compiled MERIS BSA database compares well to MODIS BSA data in the NIR. Correlation coefficients for the entire year are very high (0.98) with no bias ($< 1\%$) and only small σ ($\sim$0.017 or $\sim$6%). Comparing the MERIS BSA database to GOME LER at around 760 nm leads to a lower correlation (0.80) and two clusters can clearly be identified in the corresponding scatter density plots which are related to the strong albedo contrasts along coastlines not resolved by the GOME LER as well as the underestimation of the GOME LER in arid regions in winter.

2. The largest differences between FRESCO+ MERIS BSA and FRESCO+ GOME retrievals are found for relatively small cloud fractions where the impact of the surface reflectance on the measured signal is largest. This is of particular interest because tropospheric trace gas retrievals are generally limited to small cloud fractions. The effect of the MERIS BSA dataset on the derivation of FRESCO+ cloud pressure is only minor.

3. Artefacts in cloud detection along coastlines due to the coarse resolution or water-land mismatching of the GOME LER data were successfully eliminated. This is of importance for spaceborne trace gas retrievals because inaccurate cloud parameters lead to inaccuracies in the air mass factor computations, especially in polluted regions (Boersma et al., 2004). A majority of the world's largest megacities are located in the immediate vicinity to the ocean and trace gas remote sensing retrievals are expected to be indirectly improved in these areas by incorporating the MERIS BSA database into FRESCO+. This is supported by preliminary results of NO_2 VCD_{trop} and O_3 VCD derived with the FRESCO+ MERIS cloud parameters.

4. Using the MERIS database in the FRESCO+ retrievals leads to a better agreement with HICRU for January and July 2006 on a global scale. The average difference of derived effective cloud fractions was reduced from 0.02 (0.03) to 0.00 (0.02) for the exemplary month of January 2006 (July 2006). The correlation improved from $\sim$0.92 to 0.96 and RMSE decreased from 0.08 to 0.05.

5. Comparisons to HICRU also point out that effective cloud fractions over arid regions were successfully reduced and the spatial distribution became much smoother with MERIS BSA. However, FRESCO+ MERIS effective cloud fractions over highly reflecting desert targets are still overestimated for summer months. One reason could be the presence of, or lack of accurate information about, absorbing aerosols in these areas which hampered the albedo retrieval. In addition, FRESCO+ effective cloud fractions are also very sensitive to small changes in surface reflectivity for high surface albedo values. Empirically derived correction factors might enhance the presented MERIS BSA dataset in arid regions in the future.

6. FRESCO+ MERIS also is in better agreement to HICRU in the ITCZ where FRESCO+ GOME underestimates effective cloud fraction over land due to residual cloud signatures in the surface albedo dataset.

7. SCIAMACHY NO_2 VCD_{trop} and GOME O_3 VCD derived with the FRESCO+ MERIS cloud parameters over Europe and North Africa for July 2006 underlined that the MERIS BSA data climatology has a favourable indirect effect on trace gas retrievals, especially on regional scale.

The presented albedo climatology can also be applied to other cloud parameter retrieval algorithms from the O_2 A-band, e.g. to derive cloud top albedo from the SemiAnalytical CloUd retrieval Algorithm (SACURA, Kokhanovsky et al., 2003, 2006) or from the Retrieval Of Cloud Information using Neural Networks (ROCINN, Loyola et al., 2007). Although we concentrated in this study on the NIR channels relevant for O_2 A-band cloud retrievals, MERIS also measures radiances in spectral channels at 442 nm and 490 nm which could be used for cloud retrievals in the O_2-O_2 absorption band around 477 nm (Acarreta et al., 2004) or to enhance spaceborne NO_2 retrievals. Previous studies demonstrated that using higher spatial resolution of forward model parameters can lead to more accurate estimates of NO_2 tropospheric column amount (Zhou et al., 2009, 2010). Relating MERIS black-sky albedo to MODIS around 440 nm showed similar enhancements as the comparison with GOME LER in the NIR. Furthermore, the MERIS BSA at 620 nm, 665 nm, and 681 nm can be integrated in current H_2O retrievals to consider the effect of surface reflectivity on the air mass factor (e.g. Wagner et al., 2003). However, the MERIS BSA dataset is limited due to its spectral coverage to a wavelength range between 412 nm and 885 nm. It is therefore mainly interesting for trace gases with fitting windows in this wavelength range (e.g. NO_2) but not for applications in the UV wavelengths region. The obtained improvements also have consequences for trace gas retrievals from UV/VIS sensors incorporating the FRESCO+ cloud products as suggested by the GOME O_3 VCD derived with FRESCO+ MERIS in Sect. 4.2.3. Reprocessing of SCIAMACHY FRESCO+ retrievals with the new MERIS albedo database is planned in the TEMIS project (www.temis.nl). Although we tested the applicability only on SCIAMACHY data, it is expected that similar advancements

are obtained applying the FRESCO+ algorithm to any instrument which allows an O_2 A-band cloud retrieval (e.g. GOME or GOME-2). The herein presented database is available at http://www.temis.nl/data/meris.html.

Acknowledgements. We thank ESA for providing MERIS Albedomap and SCIAMACHY data as well as NASA for providing the MODIS snow product (MOD10CM) and spatially complete surface albedo products free of charge. We like to acknowledge Thomas Wagner (Max-Planck-Institute, Mainz, Germany) for fruitful discussions and thank Ronald van der A (KNMI) for the TEMIS data processing. PW was supported by the Netherlands Space Office project "SCIA-Visie".

Edited by: D. Loyola

References

Acarreta, J. R., de Haan, J. F., and Stammes, P.: Cloud pressure retrieval using the O_2-O_2 absorption band at 477 nm, J. Geophys. Res., 109, D05204, doi:10.1029/2003JD003915, 2004.

Anderson, G. P., Clough, S. A., Kneizys, F. X., Chetwynd, J. H., and Shettle, E. P.: AFGL atmospheric constituent profiles, Tech. Rep. AFGL-TR-86-0110, Air Force Geophys. Lab, Hanscom AFB, Mass., 1986.

Boersma, K. F., Eskes, H. J., and Brinksma, E. J.: Error analysis for tropospheric NO_2 retrieval from space, J. Geophys. Res., 109, D04311, doi:10.1029/2003JD003962, 2004.

Bovensmann, H., Burrows, J. P., Buchwitz, M., Frerick, J., Noël, S., Rozanov, V. V., Chance, K. V., and Goede, A. H. P.: SCIAMACHY - Mission Objectives and Measurement Modes, J. Atmos. Sci., 56, 127-150, 1999.

Burrows, J. P., Weber, M., Buchwitz, M., Rozanov, V., Ladstätter-Weißenmayer, A., Richter, A., DeBeek, R., Hoogen, R., Bramstedt, K., Eichmann, K.-U., Eisinger, M., and Perner, D.: The Global Ozone Monitoring Experiment (GOME): Mission Concept and First Scientific Results, J. Atmos. Sci., 56, 151-175, 1999.

de Graaf, M., Stammes, P., Torres, O., and Koelemeijer, R. B. A.: Absorbing Aerosol Index: Sensitivity analysis, application to GOME and comparison with TOMS, J. Geophys. Res., 110, D01201, doi:10.1029/2004JD005178, 2005.

Emmons, L. K., Walters, S., Hess, P. G., Lamarque, J.-F., Pfister, G. G., Fillmore, D., Granier, C., Guenther, A., Kinnison, D., Laepple, T., Orlando, J., Tie, X., Tyndall, G., Wiedinmyer, C., Baughcum, S. L., and Kloster, S.: Description and evaluation of the Model for Ozone and Related chemical Tracers, version 4 (MOZART-4), Geosci. Model Dev., 3, 43–67, doi:10.5194/gmd-3-43-2010, 2010.

Fournier, N., Stammes, P., de Graaf, M., van der A, R., Piters, A., Grzegorski, M., and Kokhanovsky, A.: Improving cloud information over deserts from SCIAMACHY Oxygen A-band measurements, Atmos. Chem. Phys., 6, 163–172, doi:10.5194/acp-6-163-2006, 2006.

Gao, F., Schaaf, C. B., Strahler, A. H., Roesch, A., Lucht, W., and Dickinson, R.: MODIS bidirectional reflectance distribution function and albedo Climate Modeling Grid products and the variability of albedo for major global vegetation types, J. Geophys. Res., 110, D01104, doi:10.1029/2004JD005190, 2005.

Grzegorski, M.: Cloud retrieval from UV/VIS satellite instruments (SCIAMACHY and GOME), PhD thesis, University of Heidelberg, Germany, 2009.

Grzegorski, M., Wenig, M., Platt, U., Stammes, P., Fournier, N., and Wagner, T.: The Heidelberg iterative cloud retrieval utilities (HICRU) and its application to GOME data, Atmos. Chem. Phys., 6, 4461–4476, doi:10.5194/acp-6-4461-2006, 2006.

Hall, D. K., Riggs, G. A., Salomonson, V. V., DiGirolamo, N. E., and Bayr, K. J.: MODIS Snow-Cover Products, Remote Sens. Environ., 83(1–2), 181–194, 2002.

Herman, J. R. and Celarier, E. A.: Earth surface reflectivity climatology at 340–380 nm from TOMS data, J. Geophys. Res., 102, 28003–28011, 1997.

Jin, Y., Schaaf, C. B., Woodstock, C. E., Gao, F., Li, X., Strahler, A. H., Lucht, W., and Liang, S.: Consistency of MODIS surface bidirectional reflectance distribution function and albedo retrievals: 2. Validation, J. Geophys. Res., 108(D5), 4159, doi:10.1029/2002JD002804, 2003.

Kaufmann Y. J. and Tanré, D.: Algorithm for remote sensing of tropospheric aerosol from MODIS, NASA Algorithm Theoretical Basis Document, Product ID: MOD04, 1998.

Kaufman, Y. J., Tanré, D., Dubovik, O., Karnieli, A., Remer, L. A.: Absorption of sunlight by dust as inferred from satellite and ground–based remote sensing, Geophys. Res. Lett., 28(8), 1479–1482, 2001.

Kleipool, Q. L., Dobber, M. R., de Haan, J. F., and Levelt, P. F.: Earth surface reflectance climatology from 3 years of OMI data, J. Geophys. Res., 113, D18308, doi:10.1029/2008JD010290, 2008.

Koelemeijer, R. B. A., Stammes, P., Hovenier, J. W., and de Haan, J. F.: A fast method for retrieval of cloud parameters using oxygen A-band measurements from the Global Ozone Monitoring Experiment, J. Geophys. Res., 106(D4), 3475–3490, 2001.

Koelemeijer, R. B. A., de Haan, J. F., and Stammes, P.: A database of spectral surface reflectivity in the range 335-772 nm derived from 5.5 years of GOME observations, J. Geophys. Res., 108(D2), 4070, doi:10.1029/2002JD002429, 2003.

Koepke, P., Hess, M., Schult, I., and Shettle, E. P.: Global Aerosol Data Set, MPI Report No. 243, Max-Planck-Institut für Meteorologie, Hamburg, Germany, 1997.

Kokhanovsky, A. A., Rozanov, V. V., Zege, E. P., Bovensmann, H., and Burrows, J. P.: A semianalytical cloud retrieval algorithm using backscattered radiation in 0.4-2.4 μm spectral region, J. Geophys. Res., 108(D1), 4008, doi:10.1029/2001JD001543, 2003.

Kokhanovsky, A. A., Rozanov, V. V., Nauss, T., Reudenbach, C., Daniel, J. S., Miller, H. L., and Burrows, J. P.: The semianalytical cloud retrieval algorithm for SCIAMACHY I. The validation, Atmos. Chem. Phys., 6, 1905–1911, doi:10.5194/acp-6-1905-2006, 2006.

Kokhanovsky, A. A., von Hoyningen-Huene, W., and Burrows, J. P.: Determination of the cloud fraction in the SCIAMACHY ground scene using MERIS spectral measurements, Int. J. Remote Sens., 30(23), 6151–6167, 2009.

Krijger, J. M., van Weele, M., Aben, I., and Frey, R.: Technical Note: The effect of sensor resolution on the number of cloud-free observations from space, Atmos. Chem. Phys., 7, 2881–2891, doi:10.5194/acp-7-2881-2007, 2007.

Kuze, A. and K. Chance: Analysis of cloud top height and cloud coverage from satellites using the O_2 A and B bands, J. Geophys.

Res., 99(D7), 14481–14491, 1994.

Liu, J., Schaaf, C., Strahler, A., Jiao, Z., Shuai, Y., Zhang, Q., Roman, M., Augustine, J. A., and Dutton, E. G.: Validation of Moderate Resolution Imaging Spectroradiometer (MODIS) albedo retrieval algorithm: Dependence of albedo on solar zenith angle, J. Geophys. Res., 114, D01106, doi:10.1029/2008JD009969, 2009.

Loyola, D.: A new cloud recognition algorithm for optical sensors, IEEE International Geoscience and Remote Sensing Symposium, IGARSS, Seattle/WA, 6–10 July 1998, 572-574, 1998.

Loyola, D., Thomas, W., Livschitz, Y., Ruppert, T., Albert, P., and Hollmann, R.: Cloud properties derived from GOME/ERS-2 backscatter data for trace gas retrieval, IEEE T. Geosci. Remote, 45/9, 2747–2758, 2007.

Moody, E., King, M., Platnick, S., Schaaf, C., and Gao, F.: Spatially Complete Global Spectral Surface Albedos: Value-Added Datasets Derived From Terra MODIS Land Products, IEEE T. Geosci. Remote, 43, 144–158, 2005.

Moody, E. G., King, M. D., Schaaf, C. B., and Platnick, S.: MODIS-derived spatially complete surface albedo products: Spatial and temporal pixel distribution and zonal averages, J. Appl. Meterol. Clim., 47, 2879–2894, 2008.

Muller, J.-P.: MERIS GLOBAL LAND SURFACE ALBEDO MAPS: Algorithm Theoretical Basis Document ATBD 1.4 BRDF/ALBEDO RETRIEVAL, available at: http://www.brockmann-consult.de/albedomap/pdf/MERIS-AlbedoMap-ATBD_BRDF_Albedo-1.0.pdf (last access: October 2010), 2006.

Munro, R., Eisinger, M., Anderson, C., Callies, J., Carpaccioli, E., Lang, R., Lefevre, A., Livschitz, Y., and Albinana, A. P.: GOME– 2 on MetOp, In Proc. The 2006 EUMETSAT Meteorological Satellite Conference, Helsinki, Finland, EUMETSAT P.48, ISBN 92-9110-076-5, 2006.

Oleson, K. W., Bonan, G. B.,Schaaf, C. B., Gao, F., Jin, Y., and Strahler, A.: Assessment of global climate model land surface albedo using MODIS data, Geophys. Res. Lett., 30(8), 1443, doi:10.1029/2002GL016749, 2003.

Preusker, R., Hünerbein, A., Fischer, J., Brockmann, C., and Krämer, U.: MERIS GLOBAL LAND SURFACE ALBEDO MAPS: ATBD Cloud detection, available at: http://www.brockmann-consult.de/albedomap/pdf/atbd_cloud_detection_amap__5.pdf (last access: October 2010), 2008.

Remer, L. A., Kleidman, R. G., Levy, R. C., Kaufman, Y., J., Tanré, D., Mattoo, S., Martins, J. V., Ichoku, C., Koren, I., Yu, H., and Holben, B. N.: Global aerosol climatology from the MODIS satellite sensors, J. Geophys. Res., 113, D14S07, doi:10.1029/2007JD009661, 2008.

Richter, A., Burrows, J. P., Nüß, H., Granier, C., and Niemeier, U.: Increase in tropospheric nitrogen dioxide over China observed from space, Nature, 437, 129-132, doi:10.1038/nature04092, 2005.

Schaaf, C. B., Gao, F., Strahler, A. H., Lucht, W., Li, X., Tsang, T., Strugnell, N., Xiaoyang, Z., Jin, Y., Muller, J.-P., Lewis, P., Barnsley, M. J., Hobson, P. H., Disney, M. I., Roberts, G., Dunderdale, M., Doll, C., D'Entremont, R. P., Hu, B., Liang, S., Privette, J. L., and Roy, D.: First operational BRDF, albedo nadir reflectance products from MODIS, Remote Sens. Environ., 83, 135–148, 2002.

Schlundt, C., Kokhanovsky, A. A., von Hoyningen-Huene, W., Dinter, T., Istomina, L., and Burrows, J. P.: Synergetic cloud fraction determination for SCIAMACHY using MERIS, Atmos. Meas. Tech., 4, 319–337, doi:10.5194/amt-4-319-2011, 2011

Schroeder, T., Preusker, R., Schaale, M., and Fischer, J.: MERIS GLOBAL LAND SURFACE ALBEDO MAP, Algorithm Theoretical Document ATBD 1.2 Aerosol Correction, available at: http://www.brockmann-consult.de/albedomap/pdf/atbd_1_3_aerosol_corr_AMAP.pdf (last access: October 2010), 2005.

Spurr, R.: LIDORT and VLIDORT: Linearized pseudo-spherical scalar and vector discrete ordinate radiative transfer models for use in remote sensing retrieval problems, in: Light scattering reviews, edited by: Kokhanovsky, A., Berlin, Springer, 229-271, 2008.

Stammes, P., Sneep, M., de Haan, J. F., Veefkind, J. P., Wang, P., and Levelt, P. F.: Effective cloud fractions from the Ozone Monitoring Instrument: Theoretical framework and validation, J. Geophys. Res., 113, D16S38, doi:10.1029/2007JD008820, 2008.

Tuinder, O. N. E., de Winter-Sorkina, R., and Builtjes, P. J. H.: Retrieval methods of effective cloud cover from the GOME instrument: an intercomparison, Atmos. Chem. Phys., 4, 255–273, doi:10.5194/acp-4-255-2004, 2004.

Tsvetsinskaya, E. A., Schaaf, C. B., Gao, F., Strahler, A. H., Dickinson, R. E., Zeng, X., and Lucht, W.: Relating MODIS-derived surface albedo to soils and rock types over Northern Africa and the Arabian peninsula, Geophys. Res. Lett., 29(9), 1353, doi:10.1029/2001GL014096, 2002.

Valks, P. and R. van Oss: TOGOMI Algorithm Theoretical Basis Document, Issue 1.2, TOGOMI/KNMI/ATBD/001, KNMI/ESA, November 2003, http://www.gse-promote.org/services/ozone_nrt/togomi_ATBD_v1.21.pdf (last access: March 2011), 2003.

van der A, R. J., Eskes, H. J., Boersma, K. F., van Noije, T. P. C., Van Roozendael, M., De Smedt, I., Peters, D. H. M. U., and Meijer, E. W.: Trends, seasonal variability and dominant NO_x source derived from a ten year record of NO_2 measured from space, J. Geophys. Res., 113, D04302, doi:10.1029/2007JD009021, 2008.

Vasilkov, A., Joiner, J., Spurr, R., Bhartia, P. K., Levelt, P., and Stephens, G.: Evaluation of the OMI cloud pressures derived from rotational Raman scattering by comparisons with other satellite data and radiative transfer simulations, J. Geophys. Res., 113, D15S19, doi:10.1029/2007JD008689, 2008.

Vermote, E. F., El Saleous, N., Justice, C. O., Kaufman, Y. J., Privette, J. L., Remer, L., Roger, J. C., and Tanré, D.: Atmospheric correction of visible to middle-infrared EOS-MODIS data over land surfaces: Background, operational algorithm and validation, J. Geophys. Res., 102(D14), 17131-17141, 1997.

Wagner, T., Heland, J., Zöger, M., and Platt, U.: A fast H_2O total column density product from GOME - Validation with in-situ aircraft measurements, Atmos. Chem. Phys., 3, 651–663, doi:10.5194/acp-3-651-2003, 2003.

Wagner, T., Beirle, S., Deutschmann, T., Grzegorski, M., and Platt, U.: Dependence of cloud properties derived from spectrally resolved visible satellite observations on surface temperature, Atmos. Chem. Phys., 8, 2299–2312, doi:10.5194/acp-8-2299-2008, 2008.

Wang, P., Stammes, P., van der A, R., Pinardi, G., and van Roozendael, M.: FRESCO+: an improved O_2 A-band cloud retrieval algorithm for tropospheric trace gas retrievals, Atmos. Chem. Phys., 8, 6565–6576, doi:10.5194/acp-8-6565-2008, 2008.

Zhou, Y., Brunner, D., Boersma, K. F., Dirksen, R., and Wang, P.: An improved tropospheric NO_2 retrieval for OMI observations in the vicinity of mountainous terrain, Atmos. Meas. Tech., 2, 401–416, doi:10.5194/amt-2-401-2009, 2009.

Zhou, Y., Brunner, D., Spurr, R. J. D., Boersma, K. F., Sneep, M., Popp, C., and Buchmann, B.: Accounting for surface reflectance anisotropy in satellite retrievals of tropospheric NO_2, Atmos. Meas. Tech., 3, 1185–1203, doi:10.5194/amt-3-1185-2010, 2010.